Czech Technical University in Prague
Faculty of Nuclear Sciences and Physical Engineering

Department of Physical Electronics
Optics and nanostructures

Studium nedifraktujících svazků
Study of non-diffracting beams

Master's thesis

Author: Bc. Jan Křížek
Supervisor: doc. RNDr. Miroslav Šulc, Ph.D.
Year: 2016

Prohlášení

Prohlašuji, že jsem svou bakalářskou práci vypracoval samostatně a použil jsem pouze podklady (literaturu, projekty, SW atd.) uvedené v přiloženém seznamu.

V Praze dne ....

Bc. Jan Křížek

Poděkování

Největší poděkování patří doc. RNDr. Miroslavu Šulcovi Ph.D. za úžasnou příležitost podílet se na tomto projektu. Za jeho pomoc při vypracování práce i za podporu v těžké životní situaci. Dále pak Jean-Christophe Gaydovi za stimulující konzultace a možnost podílet se na experimentální činnosti přímo v CERN. Dík patří i Ing. Štěpánu Kuncovi za pomoc při experimentech s interferometrií. V neposlední řadě i institucím TOPTEC a CERN, které celý projekt zaštiťují a bez jejichž finanční podpory by realizace nebyla možná. A nakonec rodině: Janě, Vladimírovi, Martinovi a Haně, kteří mě podporovali po celou dobu studií a vychovali ve mě člověka toužícího po poznání.

Ackowledgement

The highest gratitude belongs to doc.RNDr. Miroslav Šulc Ph.D. for the wonderful opportunity to participate in this project. For his assistance in drafting work and for his support in the difficult life situation. Furthermore, I would like to thank Jean-Christoph Gayde for stimulating consultations and the opportunity to participate in experimental activities in the CERN. Thanks belong also to Ing. Štěpán Kunc for his help within interferometry experiments. Last but not least, institutions CERN and TOPTEC for the project sheltering and without whose financial support the realisation would not be possible. And finally, to my family: Jana, Vladimir, Martin and Hana who supported me throughout all studies and raised up in me a person yearning for knowledge.

Bc. Jan Křížek

Název práce:
Studium nedifraktujících svazků

Autor: Bc. Jan Křížek

Specializace: Optics and nanostructures

Druh práce: Master's thesis

Vedoucí práce: doc. RNDr. Miroslav Šulc, Ph.D.
TOPTEC: Turnov Optoelectronic research center,
Institute of Plasma Physics of the Czech Academy of Science, v.v.i.

Konzultant: Jean-Christophe Gayde
The Experiment Metrology unit,
EN/MEF-SU Large Scale Metrology section,
CERN

Konzultant: prof. Ing. Jiří Čtyroký, DrSc.
Institute of Photonics and Electronics of the CAS,
Academy of Sciences CR, v.v.i.

Abstrakt: **Práce pojednává o generaci a využití nedifrakčních optických svazků. Je podán výklad o vzniku a vlastnostech besselovských paprsků a možnostech jejich využití v interferometrii. Je předložen teoretický rozbor a výsledky simulací, ilustrující několik nových vlastností při interferenci besselovského svazku s gaussovským svazkem a dále dvou besselovských svazků. Součástí je také teoretický rozbor generace nedifrakčních svazků na dlouhou vzdálenost pomocí optických vad.**

Klíčová slova: nedifraktivní svazky na dlouhé vzdálenosti, besselovksé svazky, interferometrie, metrologie, počítačové simulace nedifraktivních svazků

Title:
Study of non-diffracting beams

Author: Bc. Jan Křížek

Abstract: **The thesis deals with the generation and use of non-diffracting optical beams. We submit the analysis of Bessel beams and their possibilities in interferometry. We refer to new features for the interference of the Bessel beam plus the Gaussian beam and further the interference of two Bessel beams. We also propose the study of long range non-diffracting beams generator via optical aberrations.**

Key words: non-diffracting beams, long range non-diffracting beams, Bessel beams, interferometry, metrology, computer simulations of non-diffracting beams

Tuto práci věnuji svému tatínkovi, který vždy statečně uměl najít světlo i tváří v tvář nejhlubší temnotě.

Contents

Introduction **14**

1 Optical beams **15**

1.1 Introduction to Non-diffracting waves 15

1.2 General wave equation 16

1.2.1 Spectral function 16

1.3 Light field propagation - VirtualLab Fusion 18

1.3.1 Ray tracing 18

1.3.2 Field tracing 18

1.4 Gaussian beam 21

1.4.1 Parameters of the Gaussian beam 21

1.5 Bessel beam as mathematical construct 24

1.5.1 Introduction to Bessel beams 24

1.5.2 Scalar solution of a Bessel Beam 24

1.5.3 Parameters of a Bessel beam 25

2 Interferometry with Non-diffracting beams **28**

2.1 Bessel beam generation 28

2.1.1 Bessel beams generated by an axicon 30

2.1.2 Transversal characteristic 31

2.1.3 Longitudinal characteristic 34

2.2 Conclusions and beams comparison 35

2.3 Plane - Plane interferometry 38

2.3.1 Simulation 39

2.3.2 Experiment 40

2.4 Bessel - Plane interference 41
2.4.1 Simulation 41
2.4.2 Experiment 46
2.5 Bessel - Bessel interference 47
2.5.1 Degrees of freedom 47
2.5.2 Combination of misalignments 49
2.5.3 Experiment 51
2.5.4 Model situation of absolute distance measurement 51
2.6 Structured field + Plane interference 54

3 Long range non-diffracting beams **55**
3.1 Long range non-diffracting beam generation 55
3.1.1 Axicon generalization 55
3.1.2 Non-diffracting beams generated by a spherical aberration . . 56
3.2 Design of long range non-diffracting beam generator 56
3.2.1 Phase function of ND generator 56
3.2.2 Wavefront distortion described by Zernike polynomials 57
3.3 Long range non-diffracting beam generator 59
3.3.1 Simulation 59
3.3.2 Experiment 60
3.4 Long range non-diffracting beams conclusion 60

Conclusion **62**

Bibliography **63**

List of Figures

1.1 Vectorial relations 17

1.2 Angular spectrum of Bessel beam and Gaussian beam 18

1.3 Propagation of the field through an optical system 19

1.4 Gaussian Beam propagation scheme 22

1.5 Gaussian Beam simulation of the longitudinal phase distribution. . . 23

1.6 *a)* Generation of J_0 beam by spatially unlimited plane waves; *b)* Generation of J_0 beam by spatially limited plane waves 25

1.7 Bessel beam propagation scheme 26

1.8 Bessel beam transversal amplitude and phase characteristic 27

2.1 Creation of a Bessel beam with an annular slit and lens 29

2.2 Creation of a Bessel beam with an axicon 30

2.3 The scheme of Bessel beam created by an axicon 30

2.4 Simulation of the transversal intensity distribution of the Bessel beam generated by the Axicon and incoming Gaussian beam. 32

2.5 Experimental investigation of the transversal intensity distribution of the Bessel beam generated by the Axicon and incoming Gaussian beam. 33

2.6 Simulation of the longitudinal intensity distribution of the Bessel beam generated by the Axicon and incoming Gaussian beam. 34

2.7 Simulation of the longitudinal intensity distribution of the Bessel beam generated by the Axicon and incoming Plane wave. 34

2.8 Experimental investigation of the longitudinal intensity distribution of the Bessel beam generated by the Axicon and incoming Gaussian beam. 35

2.9 Comparison of Gaussian and Bessel beams 37

2.10 Scheme of the interference of two plane waves. 38

2.11 Interference of two plane waves. 39

2.12 Interference of two co-linear plane waves 39

2.13 Interference of two tilted plane waves 40

2.14 Interference of two tilted plane waves with different relative phase shift; *a)* Michelson interferometer *b)* camera image *c)* Intensity in the single point while inducing relative phase shift 40

2.15 Interference of a Bessel beam and plane wave; *a)* Bessel - plane interference *b)* Bessel - shifted plane interference (longitudinal misalignment) *c)* angular misalignment 41

2.16 *a)* Longitudinal and *b)* transversal phase characteristic of a Bessel beam *c)* Interference of artificial plane waves 41

2.17 Camera image in false colors. Bessel - Collinear Plane interference transversal intensity profile. 42

2.18 Simulation Bessel - Collinear Plane interference longitudinal intensity profile. Plane wave phase delay $0 - 1.5\ \mu m$. 42

2.19 Simulation Bessel - Collinear Plane interference transversal intensity profile. Relative phase delay $0 - \lambda = 600nm$. 43

2.20 Bessel beam + Tilted plane wave interference. 43

2.21 Integral value of the interference contrast for different Bessel:Plane intensity ratios. Coordinate dependant interference contrast. 44

2.22 Simulation Bessel - Plane interference. 45

2.23 Modified Mach - Zehnder interferometer for the Bessel+Plane interference. 46

2.24 Measured Bessel Plane interference point intensity fluctuation while the relative phase shift is induced. 46

2.25 Measured Bessel Plane interference integral intensity fluctuation while the relative phase shift is induced. 46

2.26 Interference of two Bessel beams. 47

2.27 Simulation of the interference of two collinear Bessel beams with inducing relative phase shift $0 - \lambda$ 47

2.28 Simulation of Interference of two mutually tilted Bessel beams. 48

2.29 Simulation of tips offset of two interfering Bessel beams. 49

2.30 Simulation of the combination of angular misalignment and relative phase shift. 49

2.31 Simulation of the combination of tips offset and relative phase shift. . 50

2.32 Simulation of the combination of tips offset and angular misalignment. 50

2.33 Simulation of the combination of tips offset, angular misalignment and relative phase shift. 50

2.34 Experiment of the interference of two Bessel beams. 51

2.35 Concept of absolute distance z measurement with two interfering Bessel beams 52

2.36 The position of the first minimum z_{1min} related to the axicon angle α of Bessel beams and their mutual propagation angle θ. 53

2.37 Simulation of absolute distance z measurement with two interfering Bessel beams. 53

2.38 Interference of structured fields with plane wave. 54

3.1 Concept of the long range non diffracting beam generation 56

3.2 Phase retardation function of the non-diffracting beam generator . . . 57

3.3 First 16 Zernike polynomials 58

3.4 Zernike polynomials with the rotational symmetry 58

3.5 Scheme of long range non diffracting beam generator 59

3.6 Wavefront outgoing from the non-diffracting beam generator. 59

3.7 Long range non-diffracting beam simulation 60

3.8 Camera image showing long range non-diffracting beam in comparison with Gaussian beam 61

List of symbols

A	positive spectral constant related to the initial boundary condition
$A_n(k_\rho, k_z, \nu)$	spectral function of cylindrical coordinate system
α	axicon angle of a Bessel beam
β	Gaussian beam divergence
C	radius of curvature of a wavefront
d	the distance between two interferring Bessel beams cores
$\Delta\rho$	Bessel beam central core radius
ϵ_r	relative permittivity
γ	axicon angle of axicon
$I(r)$	intensity of light
$J_0(x)$	the position of the Bessel function zeros
$J_n(k_\rho\rho)$	n-order Bessel function
k_ρ, k_z	wave vectors
Λf	the distance of Bessel beams cores for relevant minima
λ	wavelength of light
$\mathbf{E}(\mathbf{r})$	the complex amplitudes of the harmonic electric field
$\mathbf{H}(\mathbf{r})$	the complex amplitudes of the harmonic magnetic field
$\mathcal{P}_{\Delta z}$	matrix operator of the field
n	idex of refraction
ν	spatial frequency
ω	time frequency of electric field amplitude
$\Phi(z)$	Gouy phase shift
$\psi(\rho, z, t)$	field function
R, D	radius resp. diameter of incoming beam or optical element
ρ	transversal coordinate $\rho^2 = x^2 + y^2$
(ρ, Φ, z)	cylindrical coordinate systém
t	time
θ	angle between two interferring beams
$\Theta(\rho)$	phase function of optical element
$w(z)$	Gaussian beam width at z
w_0	Gaussian beam waist radius
$\widehat{e_i}$	electric field polarisation state
(x, y, z)	axis of cartesian coordinate systém
z_{1min}	the z position of the first minima of two interferring Bessel beams
z_{max}	length of a Bessel beam
Z_n	index of Zernike polynomial
z_R	Rayleigh range

Introduction

Non-diffracting fields are relatively new topic in contemporary optics. Since the milestone Durnin's article was published in 1987, it has been subject of vivid research: google scholar responds with over 30 000 results while finding the keyword "non-diffracting beams". These fields can yield special properties which have not been observed before, such as resistance against divergence, non-rectilinear propagation or self-healing property after they pass an obstacle. This peculiar behaviour has found many applications, however, its potential is far from being exhausted.

In this work, we turned our interest onto possibilities of these beams in optical metrology. Finding new methods of measurements is required task in case of very precise experiments held in CERN. Especially, large-scale experiments are the very demanding challenge that has no parallel in any other engineering practice. Implementing approaches based on laser technology seems to be an ideal candidate for this purpose, however, they facing significant limits caused by a beam spreading. Non-diffracting beams might be useful tool for mitigating limiting factors and so they are in the particular interest of *The Experiment Metrology unit* under *Large Scale Metrology section* in CERN.

Activity under this thesis was aimed onto the interferometry with Bessel beams and the long-range non-diffracting field generation. The work includes theoretical and experimental analysis of given topic supported by optical simulations made in software VirtualLab Fusion. We are dealing with the brand new field of interest, so the most of the physical assumptions are authorial and has not been published before.

The thesis is organised as follows:

- **Chapter 1** is devoted to the theoretical background of Bessel beams - the best-known representative of non-diffracting beams. We present basic equations and we put side by side conventional Gaussian beam with the Bessel beam.
- **Chapter 2** deal with the interference of a Bessel beam with a Gaussian beam and further of two Bessel beams. We present simulations and the physical explanation of results observed by experiments.
- **Chapter 3** propose a new approach to an understanding of long-range non-diffracting beams generator by means of optical aberrations, with the help of established theory of Zernike polynomials.

Chapter 1

Optical beams

1.1 Introduction to Non-diffracting waves

When considering the light wave propagation it is convenient to investigate whether there can exist a light wave which is spatially limited and propagates in one significant direction. In that case, we call them light beams. For example the well-known *plane wave* can not be considered as a beam even though it propagates in only one direction; its energy is infinite and it is not spatially limited. In contrast, *a spherical wave* comes from a single point, but "diverges" in all directions. We are interested in the waves which have the normal of the weave-fronts oriented in some given direction, such waves are called paraxial waves and they have to come from the solution of the wave equation. The best known paraxial beam is Gaussian beam and its higher modes [1].

Beams or light pulses are subject to the phenomena of diffraction. In the modern treatment, any wave propagating in a media is affected by the diffraction causing its spatial broadening. That has shown to be a natural property of every wavefield. For the application in optics it means that wherever transverse localization is needed, this effect is limiting. That is a case of image forming, free space communications, optical lithography or optical tweezers.

In optics, there exist several ways how to preserve transversal shape over long distances, for example by bonding light into a waveguide. However, it is convenient to ask how this behaviour can be mitigated or even suppressed in the free-space propagation. This concept has been investigated both theoretically and experimentally and solutions fulfilling these conditions are called *non-diffracting beams*. It has been presented solutions with various peculiar behaviour such as non-rectilinear spreading (*Airy beams*), diffraction-free spreading *Bessel beam* etc [2].

1.2 General wave equation

Every existing physical wave can be described by the differential equation known as homogeneous wave equation [2].

$$\left(\frac{\partial^2}{\partial x^2}+\frac{\partial^2}{\partial y^2}+\frac{\partial^2}{\partial z^2}-\frac{1}{c^2}\frac{\partial^2}{\partial t^2}\right)\psi(x,y,z;t)=0 \tag{1.1}$$

Which can be written in the cylindrical co-ordinates $(\rho,\Phi,z;t)$ and assuming axially symmetric solutions $(\rho,z;t)$ then the equation becomes:

$$\left(\frac{\partial^2}{\partial \rho^2}+\frac{1}{\rho}\frac{\partial}{\partial \rho}+\frac{\partial^2}{\partial z^2}-\frac{1}{c^2}\frac{\partial^2}{\partial t^2}\right)\psi(\rho,z;t)=0 \tag{1.2}$$

Where $\rho^2=x^2+y^2$ The solution in the free space can be written in terms of a Bessel-Fourier transform of the variable ρ, and two Fourier transforms of variables z,t [2].

$$\psi(\rho,z,t)=\int_0^\infty \mathrm{d}k_\rho\int_{-\infty}^\infty \mathrm{d}k_z\int_{-\infty}^\infty \mathrm{d}\nu k_\rho A_n(k_\rho,k_z,\nu)J_n(k_\rho\rho)\mathrm{e}^{ik_z z}\mathrm{e}^{i\nu t} \tag{1.3}$$

where $J_n(k_\rho\rho)$ are n-order Bessel functions and $A_n(k_\rho,k_z,\nu)$ is the Fourier transform of $\psi(\rho,z;t)$. The relation among k_ρ,k_z,ν can be derived by the substitution of *Eq.(1.3)* to *Eq.(1.2)*.

$$\frac{\nu^2}{c^2}=k_\rho^2+k_z^2 \tag{1.4}$$

With this condition becomes *Eq.(1.3)* into the general solution to the wave equation *Eq.1.2*

$$\psi(\rho,z,t)=\int_0^{\frac{\nu}{c}}\int_{-\infty}^\infty k_\rho J_n(k_\rho\rho)\mathrm{e}^{iz\sqrt{\nu^2/c^2-k_\rho^2}}\mathrm{e}^{-i\omega t}S(k_\rho,\nu)\mathrm{d}k_\rho\mathrm{d}\nu \tag{1.5}$$

where $S(k_\rho,\nu)$ is the chosen spectral function typical for each solution. This general solution is frequency dependent so it yields to an expression for both beams or pulses. In this thesis we are particularly interested in the frequency independent solutions which are further elaborated in *Sections 1.4 and 1.5*

1.2.1 Spectral function

Behaviour of optical beams can be described by mean of so-called *angular spectrum*. Under angular spectrum representation, we understand the series expansion of an arbitrary field in terms of plane waves with variable amplitudes and propagation directions [3]. This idea is convenient as it reveals physical behaviour and it is unique for each solution .

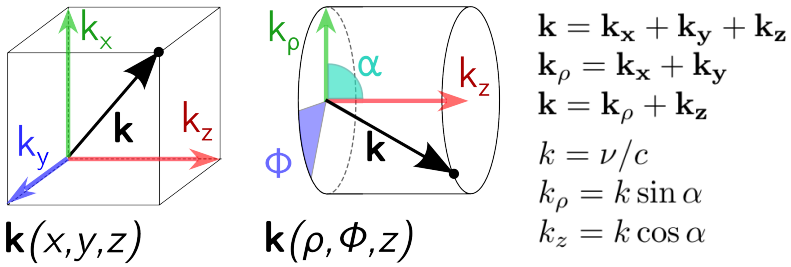

Figure 1.1: Vectorial relations

The Gaussian spectral function

In laser physics a very common shape of the beam is the Gaussian beam, which can be described by the spectral function [2]:

$$S(k_\rho, \nu) = 2A^2 \mathrm{e}^{-A^2 k_\rho^2} \delta(\nu - \nu_0) \tag{1.6}$$

Where A is a positive constant related to the initial boundary condition.

Fig.1.2a shows up the graphical interpretation of the solution *Eq.1.5* with the Gaussian spectral function as a superposition of plane waves. It corresponds with the fact, that the Gaussian beam has its most intense part along the axis of propagation. However waves are spreading into all directions (always with $(k_z \geq 0)$. *Fig.1.2b* Illustrates the angular spectral function which is in the case of Gaussian function (and only) same as its intensity distribution. Features of the Gaussian beam will be further discussed in the *Section 1.4*

The Bessel beam spectral function

Let us consider the spectral function [2]:

$$S(k_\rho, \nu) = \frac{\delta(k_\rho - \frac{\nu}{c} \sin \alpha)}{k_\rho} \delta(\nu - \nu_0) \tag{1.7}$$

The solution of *Eq.1.5* with the spectral function *Eq.1.7* comply to the graphical interpretation illustrated on *Fig.1.2c*. It is shown, that the Bessel beam is the result of the superposition of plane waves whose wave vectors draw the surface of a cone. The angular spectrum of the beam can be then described as a ring function *Fig.1.2b*. The coherent superposition of such plane waves arises as an interference field whose relative phase differences remains unchanged during the propagation and thus the transverse profile remains the same. More comprehensive description of the Bessel beam will be given in the *Section 1.5*.

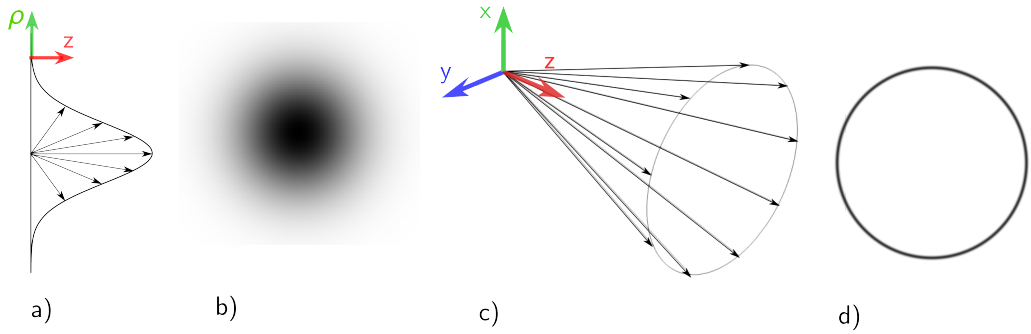

Figure 1.2: *a)* Gaussian beam decomposition to *k-vectors*; *b)* the angular spectrum of a Gaussian beam); *c)* Bessel beam decomposition to *k-vectors*; *d)* the angular spectrum of a Bessel beam

1.3 Light field propagation - VirtualLab Fusion

This section describes the basics of modelling methods used in software VirtualLab Fusion [4] [5]. The software is well suited for modelling of nondiffracting fields since it considers all features of light given by physical optics. The software was launched in 2014 by the company Wyrowski Photonics UG and provide a new technology, promising a fast electromagnetic field solver.

1.3.1 Ray tracing

In optics, we often seek for the field properties in space. It has been a longstanding experience to use geometrical optics for the purpose of propagation between two points. Regarding rays, we mathematically give them only two qualities: *direction vector and position*. The fundamental nature of rays can be concluded from the Fermat's principle. The propagation in a homogeneous media follows straight lines and it undergoes the basic laws of reflection and refraction between two different media. We assume that a ray wavelength is infinitely small and thus we neglect the wave properties of light. It has been presented a few software which uses so-called *ray tracing* approach conveniently for a variety of problems (Zemax, Code V, OSLO).

1.3.2 Field tracing

Recently, it is growing demand for more comprehensive propagation models. The wave character of light is a key factor to the final form of the field. The limitations of ray optics have become more apparent together with new possibilities and more complex components.

Maxwell's equations

The basic formulation of light like any other electromagnetic field is given by Maxwell's equations. We assume wave in the dielectric medium which is optically linear,

isotropic and non-magnetic. Then the equations have the form [1]

$$\nabla \times \mathbf{E}(\mathbf{r}) = -i\omega_0\mu_0\mathbf{H}(\mathbf{r}) \tag{1.8}$$

$$\nabla \times \mathbf{H}(\mathbf{r}) = -i\omega_0\epsilon_0\epsilon_r(\omega_0)\mathbf{E}(\mathbf{r}) \tag{1.9}$$

$$\nabla \cdot \mathbf{B}(\mathbf{r}) = 0 \tag{1.10}$$

$$\nabla \cdot \mathbf{E}(\mathbf{r}) = 0 \tag{1.11}$$

Where $\mathbf{E}(\mathbf{r})$ stands for a complex amplitude of harmonic electric field with the frequency ω_0, correspondingly for the magnetic field $\mathbf{H}(\mathbf{r})$. Dielectric features are described by relative permittivity ϵ_r.

Under given conditions, all electromagnetic components of the field can be derived once we determine the field vector [5].

$$\mathbf{f}(\mathbf{r}) = [\mathbf{E_x}(\mathbf{r}), \mathbf{E_y}(\mathbf{r})] \tag{1.12}$$

It rises from the combination of *Eq.1.8-1.11.*

For the comprehensive optical design, the model has to provide access to all parameters of the field, also taking into consideration polarisation, coherence or spectral features. It also should work with wave phenomena of the light such as interference and diffraction. Further, it should take into account Fresnel laws at boundaries between two media.

We noted that the problem of the field determination converges to the problem of finding the vector *Eq.1.12*. It still carries an information about whole 3D space, albeit one is usually interested in the distribution in transversal subsets of this space [5]. An example is given by the *Figure 1.3*. Basically, we have two types of problems: propagating in the homogeneous media and the second: modification caused by intersections when one media changes to another in an optical component. It is convenient to introduce *propagation operators* which mathematically describe how the field is influenced by its propagation between two subsets of the space [4].

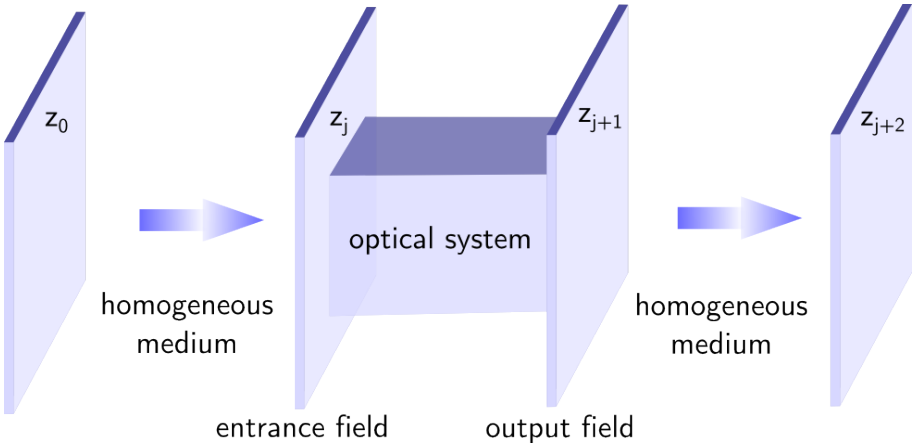

Figure 1.3: Propagation of the field through an optical system

Propagating through a homogeneous medium

Propagation through a homogeneous medium, which might be for example free space, is illustrated between planes z_0 - z_j and z_{j+1}-z_{j+2} of the *Figure 1.3*. It can be mathematically expressed by the operator equation:

$$f(x, y, z_j) = \mathcal{P}_{\Delta z} f(x, y, z_0) \tag{1.13}$$

Where the $\mathcal{P}_{\Delta z}$ is 2×2 matrix operator. Thanks to isotropy of homogeneous media it leads to a diagonal matrix which mathematically represents there are no preferred directions or the field components crosstalks. Formulation of $\mathcal{P}_{\Delta z}$ depends on the applied models developed from the scalar theory [3] and it can be fitted for certain situations [4].

- The Spectrum Plane Waves (SPW) integral
- The Rayleigh-Sommerfeld integral
- The Fresnel integral - only for paraxial fields
- The far-field approximation of SPW
- Geometrical optics - ray tracing with the field representation of complex amplitudes

Propagation through components

Now, we are investigating the influence of the area between z_j and z_{j+1}. The entrance field is modified by the intersection between two media of different index of refraction - for example, one side of the lens. We can use the similar mathematical expression for the problem as was noted in *Eq.1.13*. In this situation we can not use the simplification of isotropy and the operator $\mathcal{P}$ is generalised to full 2×2 matrix form. Consequently, we get too many variables and a determination of the field become too heavy.

One example of a representation of such operator could be the Jones matrix, then components influence only a polarisation state and the matrix consists of complex numbers. In the case of more general components for an evaluation, we would need rigorous techniques based on the grating theory or finite elements which are numerically very demanding and time-consuming.

A novel approach used by the software VirtualLab Fusion is based on smart ray tracing. It combines advantages of ray tracing with physical optics in the concept called *smart rays* [4].

- Smart rays held the full electromagnetic field information at their position - amplitudes and phases of all electric and magnetic components, thus also the polarisation.

- Smart rays are indexed since they leave the source plane. It keeps the information about its neighbours which is convenient for a proper wave-front evaluation. It also makes possible to model partially spatially coherent light.
- Smart rays include wavelength information, so the temporal coherence can be taken into consideration.

The great importance of this concept lies in the capability of fast evaluation while maintaining the complexity of physical optics features.

1.4 Gaussian beam

The electric field amplitude profile of a Gaussian beam can be described by the Gaussian function. We can assume it as a transverse electromagnetic mode. It can be derived by several ways, for example by inducing the proper spectral function *Eq.1.6* to the *Eq.1.5* and assuming paraxial approximation we can get the following expression for a complex amplitude [1]:

$$\mathbf{E}(\rho, z) = E_0 \frac{w_0}{w(z)} \exp\left(\frac{-\rho^2}{w(z)^2}\right) \exp\left(-ikz - ik\frac{\rho^2}{2R(z)} - i\Phi(z)\right) \tag{1.14}$$

This equation can be determined with the knowledge of three parameters: the beam amplitude E_0 , the Rayleigh range z_R (or the beam waist w_0) and wavelength λ which are given by initial condition.

For this expression, it was used a paraxial approximation. It fails when wavefronts do not suppress approximation condition when they are tilted by more than about 30°, as it is in the case of highly focused beams .

1.4.1 Parameters of the Gaussian beam

Parameters of the Gaussian beam can be derived from following relations which are encoded in *Eq.1.14*.

Gaussian beam intensity

Intensity is the function of a radial distance ρ and a propagation distance z.

$$I(\rho, z) = I_0 \left(\frac{w_0}{w(z)}\right)^2 \exp\left(\frac{-2\rho^2}{w^2(z)}\right) \tag{1.15}$$

where $I_0 = |E_0|^2$

With the propagation distance the axial intensity decrease due to the beam spreading.

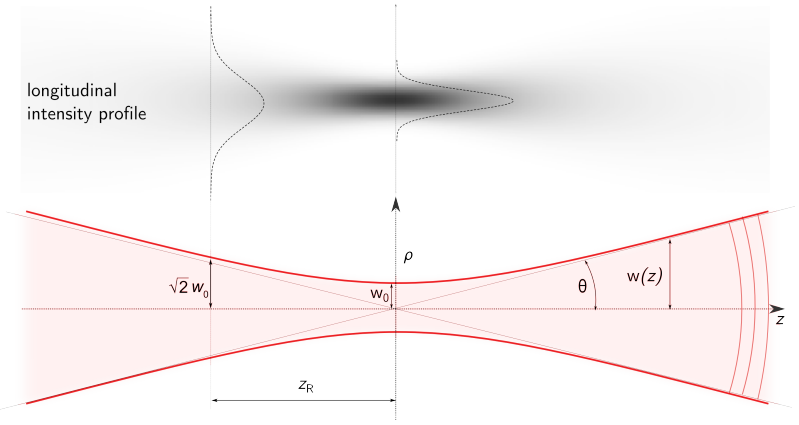

Figure 1.4: Gaussian Beam propagation scheme; w_0 beam waist size, z_R Rayleigh range, $w(z)$ beam width

Gaussian beam width

The beam profile is bounded by the value where a decrease of the beam intensity meets $1/e^2$. This area include about 86% of the overall power. It evolves with the propagation as:

$$w(z) = w_0 \sqrt{1 + \left(\frac{z}{z_\mathrm{R}}\right)^2} \tag{1.16}$$

w_0 - beam waist, determines the smallest value of the beam width. We usually set coordinates as $w(0) = w_0$.

Depth of focus and Rayleigh range

z_R in *Eq.1.16* stands for the Rayleigh range.

$$z_\mathrm{R} = \frac{\pi w_0^2}{\lambda} \tag{1.17}$$

Interval $2z_R$ around the waist is also called *focal depth* of the Gaussian beam. At the edges of the interval the beam radius has width $w(z_R) = \sqrt{2}w_0$ and the intensity is on half of its maximal value. It also determines the tolerance where we assume the beam maintain its waist profile.

Gaussian beam divergence

For the distance $z >> z_R$ the parameter $w(z)$ increases linearly. We can assume asymptotes as shown at *Fig.1.4* forming a cone like shape. The angle between axis of propagation and the asymptote is called the divergence of the beam.

$$\beta \simeq \frac{\lambda}{\pi w_0} \tag{1.18}$$

Thus for the small divergence we would need as large waist w_0 dimension as possible.

Gaussian beam phase and wavefront

The phase is given by the *Eq.1.14* members:

$$\exp\left(-ikz - ik\frac{\rho^2}{2C(z)} - i\Phi(z)\right) \tag{1.19}$$

It can be regarded as the phase of a plane wave $-ikz$ which is modified by the phase delay Φ and by the curvature of the wavefront:

$$C = C(z) = z\left(1 + \left(\frac{z}{z_0}\right)^2\right) \tag{1.20}$$

The radius of curvature is the greatest in the waist w_0 (infinite), it takes a minimum in the Rayleigh distance and then it is converging to the radius of spherical waves.

The last member of *Eq.1.19* stands for so called *Gouy phase shift*, which can be written for beams focused in both transversal dimensions as following:

$$\Phi(z) = \arctan\left(\frac{z}{z_{\mathrm{R}}}\right) \tag{1.21}$$

All waves passing through focus undergo this effect. It results in a slightly increased distance between wavefronts compared with the wavelength as defined for a plane wave. The overall phase delay for the Gaussian beam from $-\infty$ to ∞ is π.

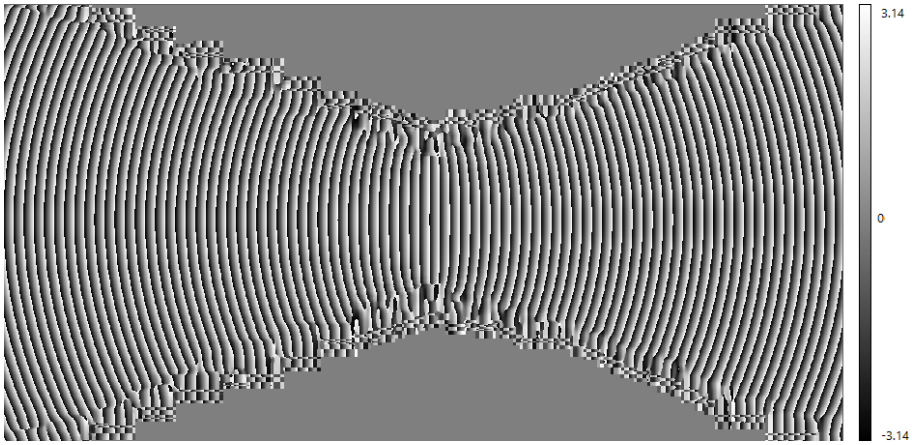

Figure 1.5: Gaussian Beam simulation of the longitudinal phase distribution. (Made in VirtualLab)

1.5 Bessel beam as mathematical construct

1.5.1 Introduction to Bessel beams

Bessel beams are the first of the family of non-diffracting beams which was investigated. Bessel beams, as a mathematical construct, was first mentioned by *Durnin* in the pioneering article from 1987 [6]. It was referred that there exist an exact solution of the homogeneous Helmholtz equation representing the beam which does not undergo transverse intensity profile spreading while propagating in a free space. Above that, they can exhibit sharply defined intensity distribution in every transverse plane on the propagation axis with the diameter of several wavelengths. Durnin's article was the milestone, it uncovered interesting field behaviour by using the scalar approximation analysis. In the same year, Durnin and his group published even experimental realisation by using the annular slit [7]. A lot of steps have been made since then - the theory has been supported by more comprehensive vectorial approaches which are exactly fulfilling the Maxwell's equations [8] and it has been described new ways of generation.

1.5.2 Scalar solution of a Bessel Beam

The general solution of the wave equation was derived in the *Section 1.2*, *Eq.1.5* and it was stated that every existing wave must yields the set of solutions and the Bessel beam is not an exception. The solution comes up in the system of cylindrical coordinates [6] [8].

The temporally independent general solution consists of a linear combination of Bessel and Neumann functions [8]. We are interested in a solution with an axial symmetry and physical meaning. Substituting the Bessel spectral function *Eq.1.7* into *Eq.1.5* we can get a following solution for the Bessel beam:

$$\psi(\rho, z, t) = \exp[i(\nu_0 t - k_z z)] J_m(k_\rho \rho) \tag{1.22}$$

It rises up that the shape of the transverse amplitude is described by the Bessel function and it is independent on the *z-axis* position, see *Fig.1.6a.*

Integral representation of a Bessel Beam

An exact solution can be written in an integral representation [6] as:

$$\psi(\rho, t) = \exp[i(\nu_0 t - k_z z)] \int_0^{2\pi} \exp[ik_\rho(x\cos\phi + y\sin\phi)] \frac{\mathrm{d}\phi}{2\pi} \tag{1.23}$$

The expression in the integral describes the angular spectrum which was pointed

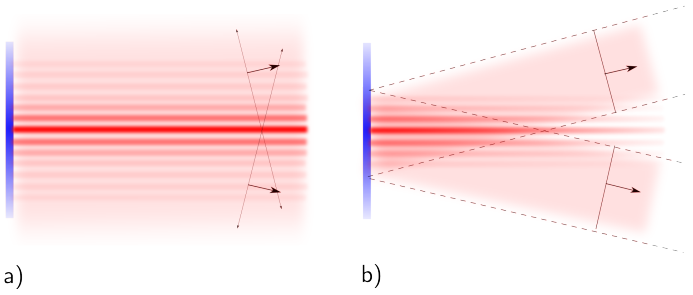

Figure 1.6: *a)* Generation of J_0 beam by spatially unlimited plane waves; *b)* Generation of J_0 beam by spatially limited plane waves

at the *Section 1.2.1*; *k-vectors* lay on the surface of the cone with an axial angle dependant on k_ρ. The non-diffracting solution comes up when the $k_\rho \neq 0$.

The mathematical features of J_m function also predicts parameters of the Bessel beam, we assume the zeroth order J_0. The function is not squared integrable, so for the physical realization of the Bessel beam over entire plane, we would need an infinite energy *Fig.1.6a*. It can be shown by the scalar diffraction theory, that we are able to generate such a beam, but over a finite area and with some concessions to the ideal one. Scheme of the generation is captured at *Fig.1.6b*. Physically realizable beams are also called *quasi*-Bessel beams (or *pseudo*).

1.5.3 Parameters of a Bessel beam

Bessel beam intensity

Normalised intensity for the J_0 is proportional to the Bessel function and it is the propagation invariant. First, observing *Fig.1.8a* illustrating intensity profile, one can see concentric rings around the sharp core. The amount of energy in each ring is equal.

$$I(\rho, z) = |A_0|^2 J_0^2(k_\rho \rho) \tag{1.24}$$

The transverse intensity profile of higher modes is given by the profile of J_m functions.

In the far field region, where the intensity pattern converges into a shape given by the angular spectrum, we can observe ring-shaped beam.

Bessel beam width

The central intensity spot radius $\Delta\rho$ is dependent on the vertex angle α. It can be derived from the first zero point of the Bessel function.

$$\Delta\rho/ = 2.405 \frac{\lambda}{\pi \sin \alpha} \tag{1.25}$$

It follows, that by increasing the vertex angle of the plane waves, see *Fig.1.7* one gets the smaller diameter of produced beam.

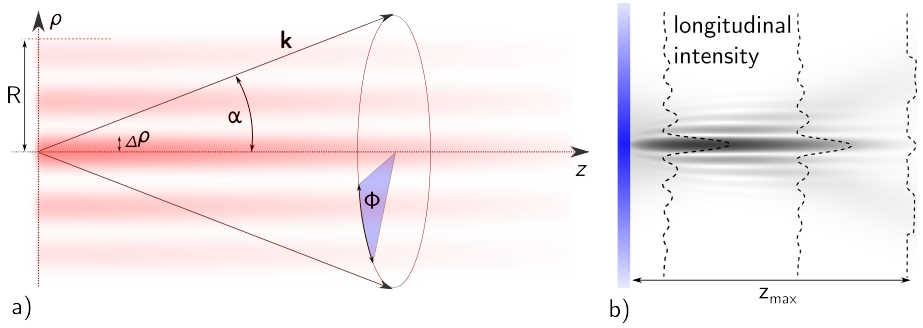

Figure 1.7: *a)*Bessel beam propagation scheme, $\Delta\rho$ central core radius, z_{max} length of a Bessel beam, α vertex angle; *b)* Longitudinal intensity profile;

Depth of focus - Bessel beam existence range

The realizable Bessel beam can exist only in the range of plane waves cross-section *Fig.1.6*. That can be geometrically given as:

$$z_{max} = \frac{R}{\tan\alpha} \tag{1.26}$$

Where R is the radius of the initial circular aperture.

Bessel beam phase distribution

The phase distribution is illustrated at the figure *1.8b)*. The coherent superposition of plane waves arises as an interference field whose relative phase differences remains unchanged during the propagation. It gives a rise to the planar phase distribution. Comparing with the intensity profile one can observe a π phase delay in neighbouring intensity rings. Circles with zero intensity belong to parts of phase jumps where the phase is not defined.

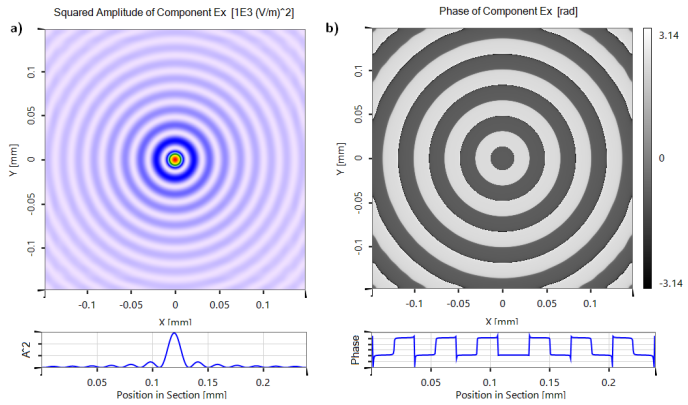

Figure 1.8: *a)* Bessel beam transversal intensity profile *b)* Bessel beam transversal phase profile. *(Made in VirtualLab)*

Chapter 2

Interferometry with Non-diffracting beams

An interferometer is a device for very precise measurements which are in principle based on an interference of light. Interferometers are usually used for a distance measurement, a determination of an index of refraction or to determine the fine structure of spectral lines in the case of interference spectroscopy. The phenomenon of interference is based on a wave summation and it is given by mutual phase differences and angles between contributing waves. An interferometry device usually compares reference beam with the signal beam which holds the information. Interference of non-diffracting beams has not been sufficiently examined and described. In 2012, it was referred on the interference of two angularly misaligned Bessel beams [16]. Further was examined the interference of two Bessel beams with a different apex angle [17]. Some work has been done with the interference light patterning for optical manipulations [18] [19]. In [20] it is shown a wave-front measurement by means of two collinear Bessel beams produced by concentric annular slits. To our best knowledge combining non-diffracting beam in a purpose of distance measurement has not been referred so far. First, we describe generation of a Bessel beam supported by simulations. Then, we investigated two types of interactions: *Bessel beam + Plane wave* and *Bessel beam + Bessel beam.*

2.1 Bessel beam generation

In the previous chapter, we discussed the theory of novel beams with some immunity to diffraction. Their peculiar behaviour has its origin in the special arrangement of the plane wave spectrum, which in the case of a Bessel beam lies on the surface of the cone. Therefore, the key to the realisation of such a beam is in assuring proper directions of contributing rays.

Annular aperture

Just after *Durnin* had published his theoretical article [6],he came up with a suggestion of realisation [7]. The illustration of the experiment is caught on *Fig.2.1*. The idea behind comes from the relation of a 2D Bessel function with a ring function through the Fourier transformation. The Fourier transformation can be optically realised by placing a transparent with an original function into the back focal plane of the lens, its Fourier image is then formed in the front focal plane.

This method of generation is rather inefficient as the most of an initial energy would not pass the transparent. In [7] it was also reported that on-axis intensity fluctuate and after the distance z_{max} it falls off rapidly. The intensity oscillation is caused by the ring slit width, as it can not be perfect ring-delta function it is subject to additional diffraction on corners.

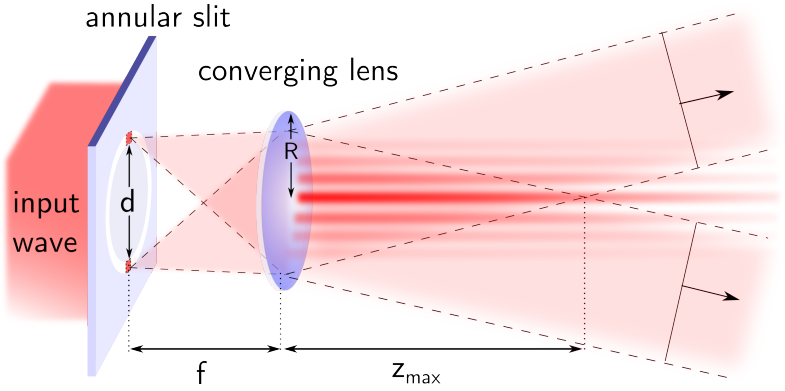

Figure 2.1: Creation of a Bessel beam with an annular slit and lens

Axicon

The Bessel beam may be created by a cone shape refraction element called an axicon *Fig.2.2* [10] [11]. Axicon can be regarded as rotationally symmetric optical wedge - incoming beam is bent into directions with circular symmetry. This approach provide us with a far more efficiency than the annular slit.

Other methods

There are a few other efficient methods of producing Bessel beams. The Beam can be transformed by passing through a holographic mask which can be static or made by spatial light modulators [12] [13]. Some other approaches benefit from circular symmetry of output from Fabry-Perot cavity [14] or special designed fiber tips [15].

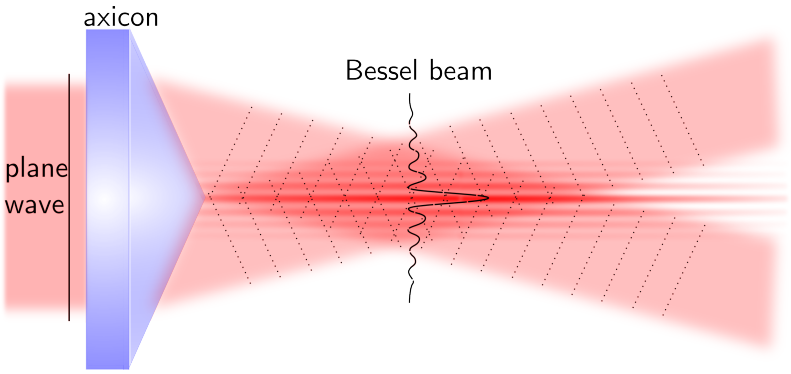

Figure 2.2: Creation of a Bessel beam with an axicon

2.1.1 Bessel beams generated by an axicon

Following section refers to simulations and experiments with Bessel Beams. We have verified theoretical predictions supported by simulations in software VirtualLab Fusion. A wavelength of light used in the simulation is $\lambda = 600$ nm. In our experiments we use the axicon *Thorlabs - AX252-A* $\alpha = 2,0°$. The He-Ne laser $\lambda = 632,8nm$ and the diameter of the incoming beam is increased by a beam expander to the $D = 1,27cm$.

Axicon has become the most widely used way of the Bessel beam generation. It has a significant advantage in its energy conversion ratio and a quality of produced beam. Moreover, an axicon is easily reachable by several commercial vendors in various modifications of diameters and cone angles.

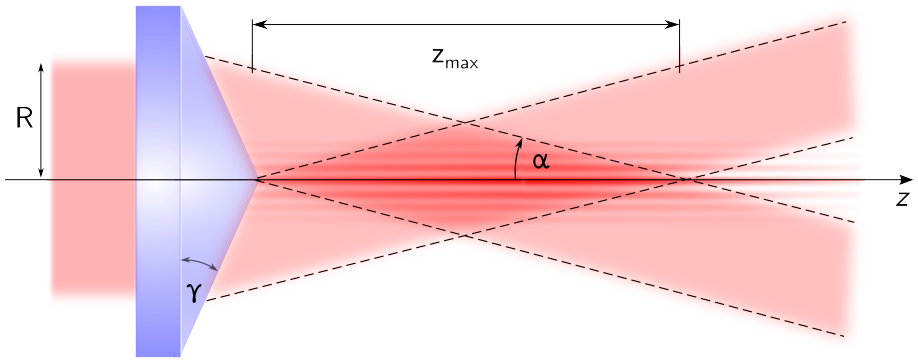

Figure 2.3: The scheme of Bessel beam created by an axicon

The top angle of the cone of plane waves depends on an architecture of an axicon. See the *Fig.2.3*

$$\alpha = (n-1)\gamma = 0.91° \tag{2.1}$$

Where n stands for the index of refraction of the material. The existence range of the Bessel beam is given by a radius of an input beam R and the axicon angle γ.

$$z_{max} \approx \frac{R}{tan(\alpha)} \approx 40\ cm \tag{2.2}$$

The size of the central spot depends on angle α of intersecting plane waves and thus on the axicon apex angle γ.

$$\Delta\rho = 2.405\frac{\lambda}{2\pi\alpha} \approx 15\ \mu m \tag{2.3}$$

2.1.2 Transversal characteristic

Simulation

Initial conditions for the axicon and input wave are following:

Input wave: Gaussian $w_0 = 6,35\ mm$, $\lambda = 632.8\ nm$, linear polarisation
Axicon: $\gamma = 2°$, $D = 25\ mm$, material: *Fused Silica* $n \approx 1.45$

First, at the area straight after the axicon contributing waves overlap only partially and the Bessel-like interference pattern arises only in the centre. *Fig. 2.4a)* We expect constant Bessel-like transversal profile over the whole range of the beam existence z_{max} *Fig. 2.4b).* After the area of the waves overlap the shape converge to the far field image, which is given by the angular spectrum. In the case of the Bessel beam we observe ring-like shape.*Fig. 2.4c),d)*

The size of the central bright core maintains its shape which is around 17 μm

Experiment

We experimentally verified previous simulations on the set-up similar to *Fig.2.3.* First image *Fig.2.5a)* shows the area where waves start overlapping. On the second picture *Fig.2.5b)* is the middle of the beam range existence. Experimental observation suffers from the limited dynamic range of the camera. Thus, we are not able to catch up sharply the bright core subsequently with much lower intense outer rings. *Fig.2.5c)* stands for the area where waves leaving their intersection area. On the *Fig.2.5d)* is the picture of the beam after 2 m and its trace on the graph paper. The last *Fig.2.5e)* shows the result on chip after instaling an objective focused on infinity, such arrangement reveals the angular spectrum.

The experimentally measured bright core belongs to 3-4 pixels which match with the size of $15 - 20\ \mu m$.

Further, on the *Fig.2.5b)* we can observe additional circular interference pattern which might be caused by the diffraction on the circular aperture during the beam collimation or by the imperfection of the axicon.

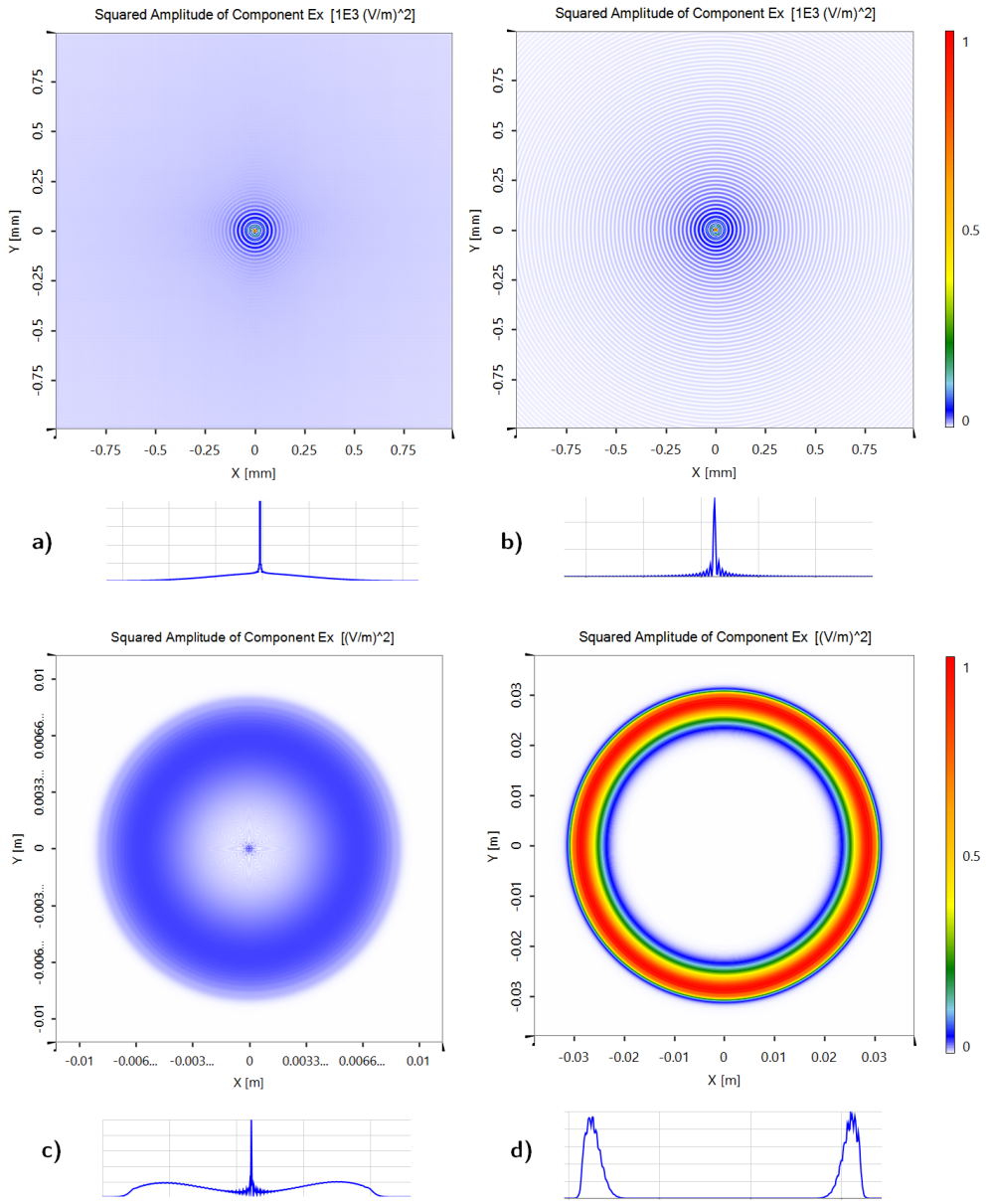

Figure 2.4: Simulation of the transversal intensity distribution of the Bessel beam generated by the Axicon and incoming Gaussian beam. When output from the axicon z=0 cm then *a)* z=1 cm , *b)* z=25 cm *c) z=50 cm d)* z=100 cm

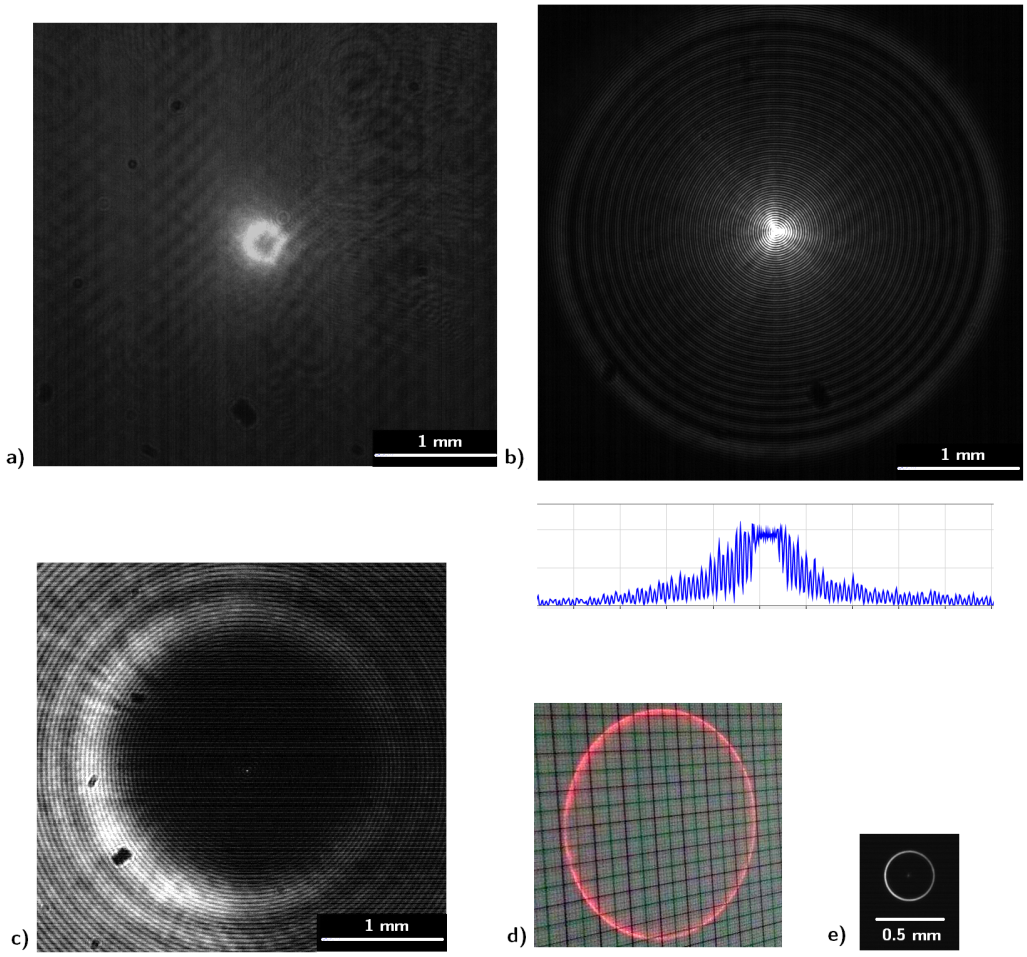

Figure 2.5: Experimental investigation of the transversal intensity distribution of the Bessel beam generated by the Axicon and incoming Gaussian beam. Further description is given in the text.

2.1.3 Longitudinal characteristic

Simulation

We are interested in the shape of the resulting structured beam in the x-z (or y-z) plane. The field is calculated in the transversal planes with a step on the z-axis and the resulting field is stitched from the line selections in the each result. Initial conditions for the simulation are following:

Input wave:	Gaussian $w_0 = 6,35\ mm$, $\lambda = 632.8\ nm$, linear polarisation
Axicon:	$\gamma = 2°$, $D = 25\ mm$, material: *Fused Silica* $n \approx 1.45$
Distance:	$z = 0 - 500\ mm$, step=$2\ mm$

The output of the simulation *Fig.2.6* reveals the Bessel beam generated on the finite area. The bright core of the Bessel function profile propagates at this distance without spreading, forming the shape of "the light-needle".

The intensity profile of the needle is given by the overlapping of input waves. If we switch the incoming beam from Gaussian beam to Plane wave, we will get the result such as in *Fig. 2.7*

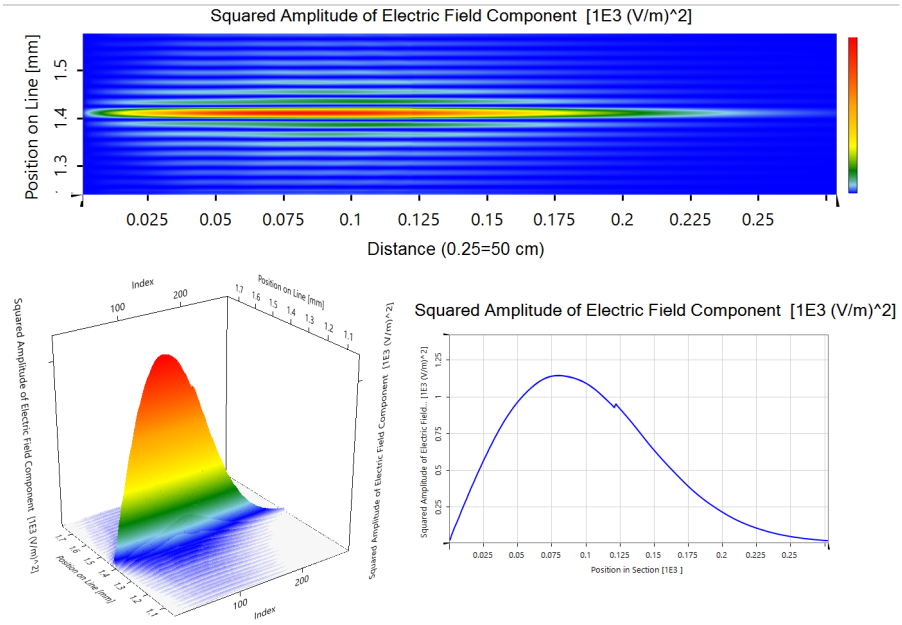

Figure 2.6: Simulation of the longitudinal intensity distribution of the Bessel beam generated by the Axicon and incoming Gaussian beam.

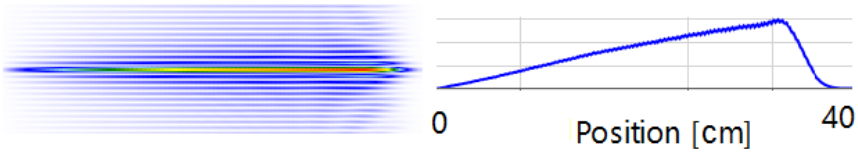

Figure 2.7: Simulation of the longitudinal intensity distribution of the Bessel beam generated by the Axicon and incoming Plane wave.

Experiment

The experimental set-up consist of the axicon Thorlabs - AX252-A = 2°. The He-Ne laser = 632,8 nm and the diameter of the incoming beam is increased by a beam expander to the D = 1,27 cm. In purpose of revealing the longitudinal beam parameters (plane *x-z*, *y-z*) we caught the transversal picture on the z-axis with 1 mm step moving from the tip of the axicon. The result *Fig.2.8* is stitched in MATLAB from the line selection in each snapshot.

We observed an obvious intensity fluctuation along the axis of propagation. This phenomenon is well described in [11]. The origin is in imperfect cone tip which can be regarded in the micro-scale rather like small lens than the sharp tip. Fluctuations represent the spatial incoherence and can be decreased by the proper circular spectral filter (analogy with pinhole spatial filtering).

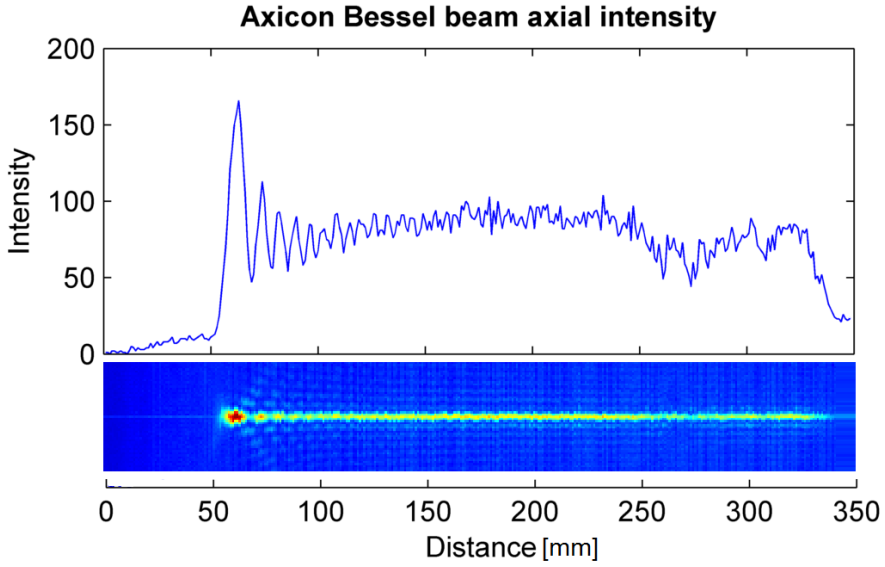

Figure 2.8: Experimental investigation of the longitudinal intensity distribution of the Bessel beam generated by the Axicon and incoming Gaussian beam.

2.2 Conclusions and beams comparison

The difference in the origin of both beams has the significant impact on its behaviour. In the *Section 1.2.1* we noted angular spectra; Gaussian beams can be emitted by an optical resonator with the spectrum of Gaussian function; Bessel beams are formed by wave vectors which lay on the surface of a cone. Gaussian beams can be also regarded as a superposition of Bessel beams with different cone angles.

Intensity profiles are given by the superposition of all contributing plane waves and give rise to the Gaussian function intensity distribution for Gaussian beams and the Bessel function intensity distribution in the case of Bessel beams.

Gaussian beams are the naturally subject to diffraction which causes the beam

spreading. It contains the most of its energy in the area where it is defined, the overall transversal energy remains the same and so with the beam spreading the point energy density decrease. In opposite Bessel beams, thanks to their special wave vector spectrum, can maintain its intensity profile over a distance of their existence. The overall beam energy is spread forming enclosing concentric rings and only a few percent contribute to the bright core, however, this enveloping energy then "feeds" the central part causing its constant profile.

In the *Fig.2.9* we present the simulation of both beams propagation with the same initial radius size of 22 μm.

- The Gaussian beam keep its transversal profile over the Rayleigh range which is 600 μm and then diverges quickly into the cone of light having after 30 cm about 5.5 mm - the beam increase its width 500 times.
- The Bessel beam keep its transversal profile over the entire range of existence. In our simulation we use the cone angel of $\alpha = 2^{\circ}$ and the initial diameter $R = 6.35$ cm, the Bessel beam length is then around 37 cm.

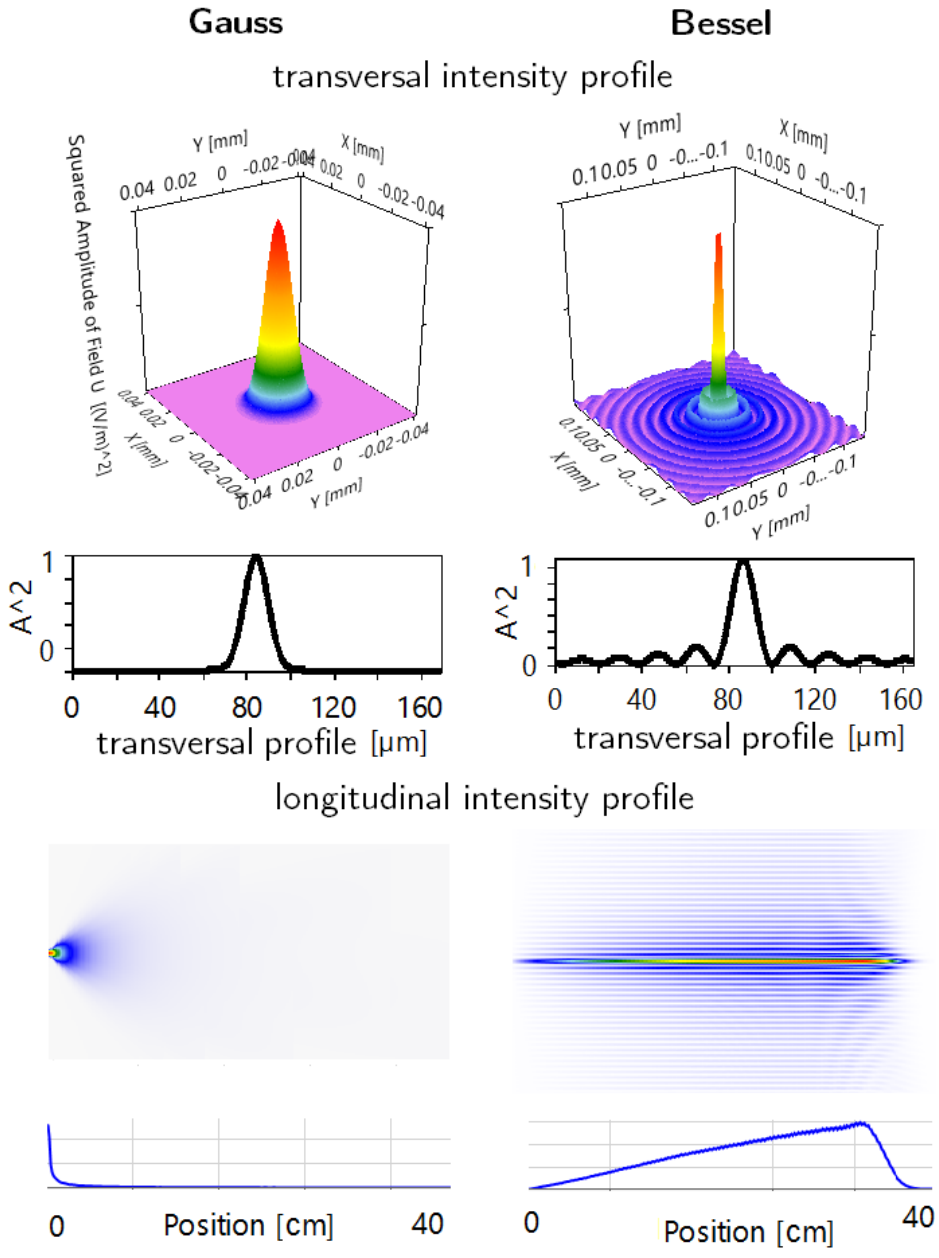

Figure 2.9: Comparison of Gaussian and Bessel beams

2.3 Plane - Plane interferometry

Gaussian beam is often approximated by plane waves which is convenient for consideration of phase behaviour. Electromagnetic plane wave is characterized by two orthogonal vector components of electric and magnetic field, oscillating in space and time. An electric plane wave is mathematically described:

$$\mathbf{E_i}(\mathbf{r}, t) = E_i \cos(\omega t - \mathbf{k_i} \cdot \mathbf{r} + \phi_i)\widehat{e_i} \tag{2.4}$$

where E_i represents the amplitude, ω stands for the time frequency, ϕ is the spatial phase, $\mathbf{k_i}$ is the wavevector and $\widehat{e_i}$ represents the linear polarization vector, and $i = 1, 2...$ are indexes of waves.

Fig. 2.10 illustrates the interference of two plane waves with propagating vectors k_1, k_2, linearly-polarized in $\widehat{e_1}, \widehat{e_2}$, monochromatic with λ, incident with angle θ respectively to the axis of propagation.

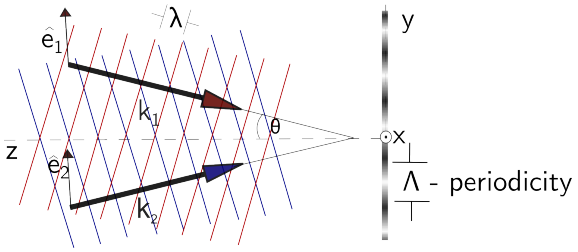

Figure 2.10: Scheme of the interference of two plane waves.

We are seeking expression for time-independent intensity distribution $I(r)$ at the intersection of two waves E_1 and E_2. Such expression can be written: $I(r) = |E_1(r) + E_2(r)|^2$ Substituting *Eq. 2.4* into previous relation we can get following interference term for fully coherent light[1]:

$$I(r) = I_0 \left[1 + \frac{2E_1E_2(\widehat{e_1}\widehat{e_2})}{I_0} \cos(\Phi(x, y)\right] \tag{2.5}$$

where the intensity term $I_0 = \frac{1}{2}(E_1^2 + E_2^2)$

The theory stated above reveals degrees of freedom of interferometry measurement given by changes induced by various misalignment. It is sensitive to the relative phase shift on the axis of waves propagation *Fig. 2.11a),b)* - the highest intensity value occurs while beams are in-phase *Fig. 2.11a)*, on the other hand the minimum intensity value belongs to the out of phase intersection *Fig. 2.11b)*. The angular detuning *Fig. 2.11c)* shows as the fringe pattern mathematically given by the *Eq.2.5*. Plane waves are theoretically characterised over entire space thus their intersection is insensitive to the transversal misalignment *Fig. 2.11d)*.

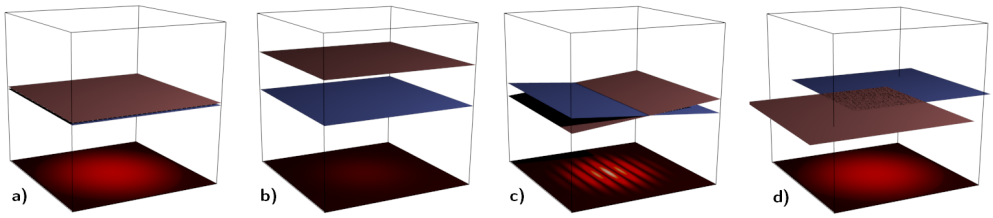

Figure 2.11: Interference of two plane waves; *a)* in-phase interference *b)* out of phase interference (longitudinal misalignment) *c)* angular misalignment *d)* transversal misalignment

2.3.1 Simulation

Intensity profile depends on the relative phase shift of interfering beams *Eq. 2.5*. While the beams are co-linear and a reference beam is phase delayed in the range of $0 - 1.5\ \mu m$ the point intensity profile follows sin function *Fig. 2.12*. For mutually tilted beams the sinusoidal fringe pattern occurs and with the reference wave phase delay, the whole pattern laterally shifts *Fig. 2.13*.

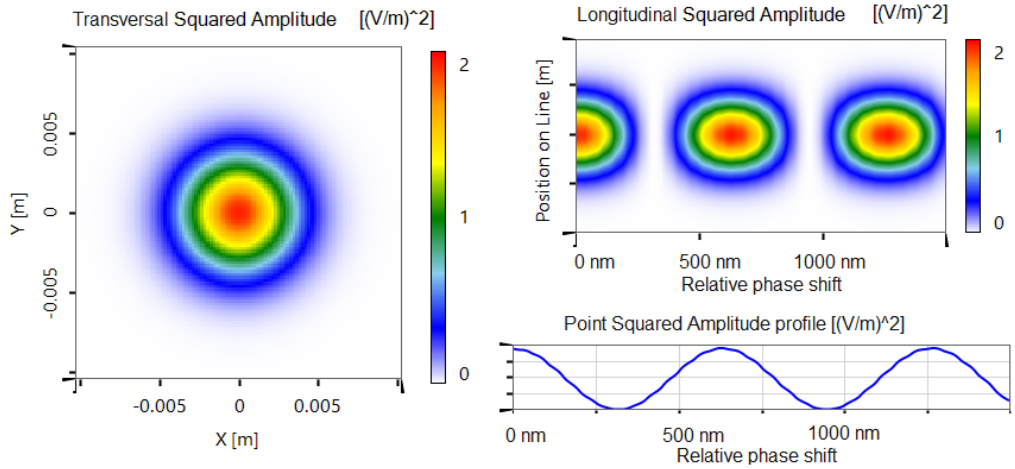

Figure 2.12: Interference of two co-linear plane waves

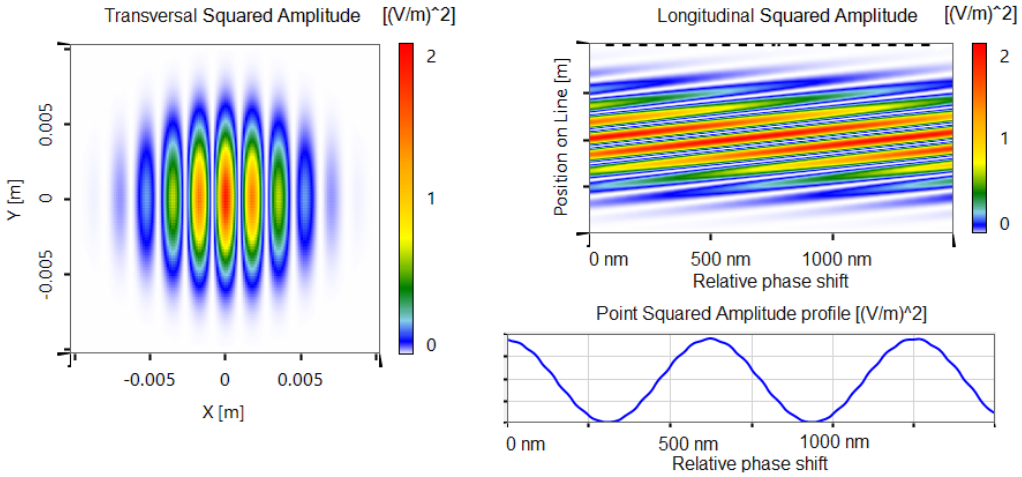

Figure 2.13: Interference of two tilted plane waves

2.3.2 Experiment

Plane - plane interference is the usual case of the classical interferometry. There are a few variations of set-ups for interferometry measurement which are commonly based on dividing wave by a beam splitter. One of the beam *signal* is influenced by a measured sample and then re-encounter with the reference beam, the intensity distribution carries the information. The most common are *Michelson interferometer* or *Mach-Zehnder interferometer*. We experimentally verified previous statements and it shows sinusoidal intensity change while the relative phase shift is induced into one arm of a Michelson interferometer. Relative phase shift was due to piezoelectric actuator movement and the results was captured by the video camera. Information was further processed in MATLAB with result in the *Fig. 2.14*.

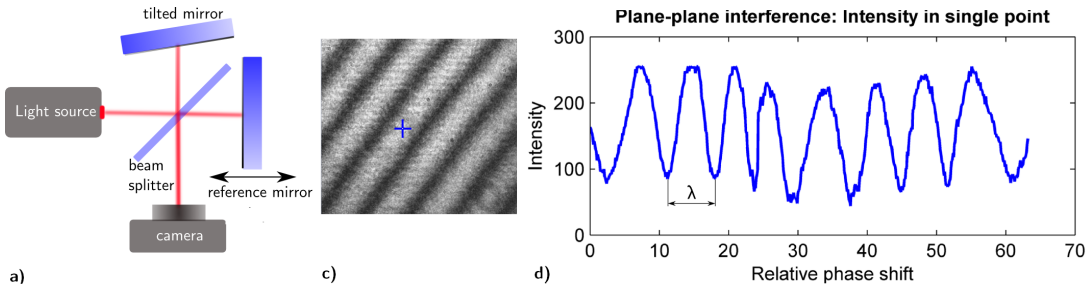

Figure 2.14: Interference of two tilted plane waves with different relative phase shift; *a)* Michelson interferometer *b)* camera image *c)* Intensity in the single point while inducing relative phase shift

2.4 Bessel - Plane interference

Previously, it was noted that a Bessel beam can be regarded as the superposition of waves which wave vectors lay on a surface of a cone *Sec.1.5*. We use this image for an illustration of Bessel beam interaction with the plane wave *Fig. 2.15*.

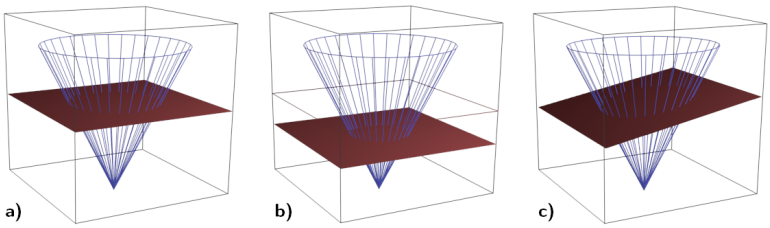

Figure 2.15: Interference of a Bessel beam and plane wave; *a)* Bessel - plane interference *b)* Bessel - shifted plane interference (longitudinal misalignment) *c)* angular misalignment

The resulting interference pattern is given by the phase characteristic of both beams. The simulation of Bessel beams phase distribution is shown on *Fig. 2.15*. A special feature of such beam is in $\lambda/2$ phase difference between neighbouring bright circles which is kept over the entire range of the beam existence. Thus, we have something like a beam with two z-axis orthogonal equi-phase plane waves which are mutually delayed by π.

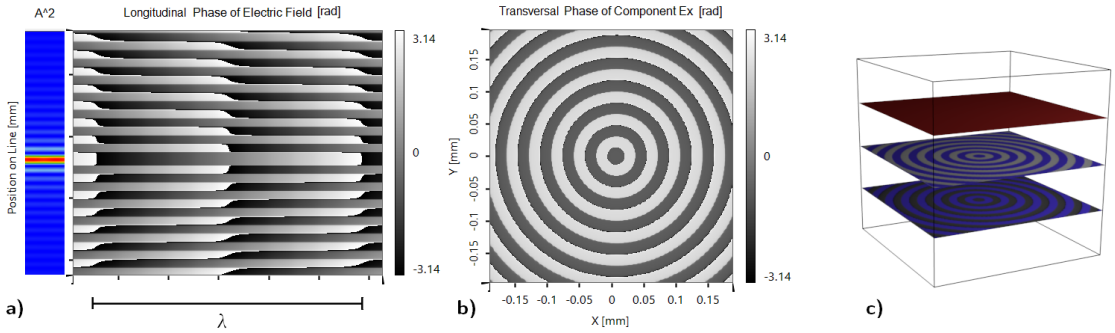

Figure 2.16: *a)* Longitudinal and *b)* transversal phase characteristic of a Bessel beam *c)* Interference of artificial plane waves

2.4.1 Simulation

Collinear interaction

While the reference plane wave encounters, it interacts in result of different intensity depending on a circle index *Fig.2.19*. Odd indexed circles including bright core have its maximal value at 0 nm and reach the minimum value at 300 nm, for even circles it is opposite. Inducing linear phase shift to the plane wave $0 - 1.5\ \mu m$ it results in the longitudinal intensity pattern which changes its character twice as often as

common (plane - plane) interference *Fig.2.18*. A minimal and maximal value of the intensity in a single point keep changing with a period corresponding to the classical interference. However, the overall intensity pattern changes its character with a double frequency. That is the new concept of a synthetic wavelength offered by the non-diffraction beams. The integral value of the overall pattern intensity is conserved since there is just opposite trend in intensity development between adjacent rings. But, if we put a threshold into our sensor, we are able to detect just the moment when the integral intensity reaches some value, and that is within twice frequency.

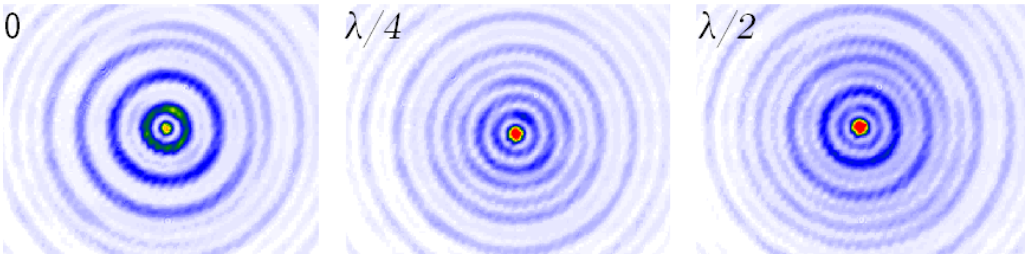

Figure 2.17: Camera image in false colors. Bessel - Collinear Plane interference transversal intensity profile.

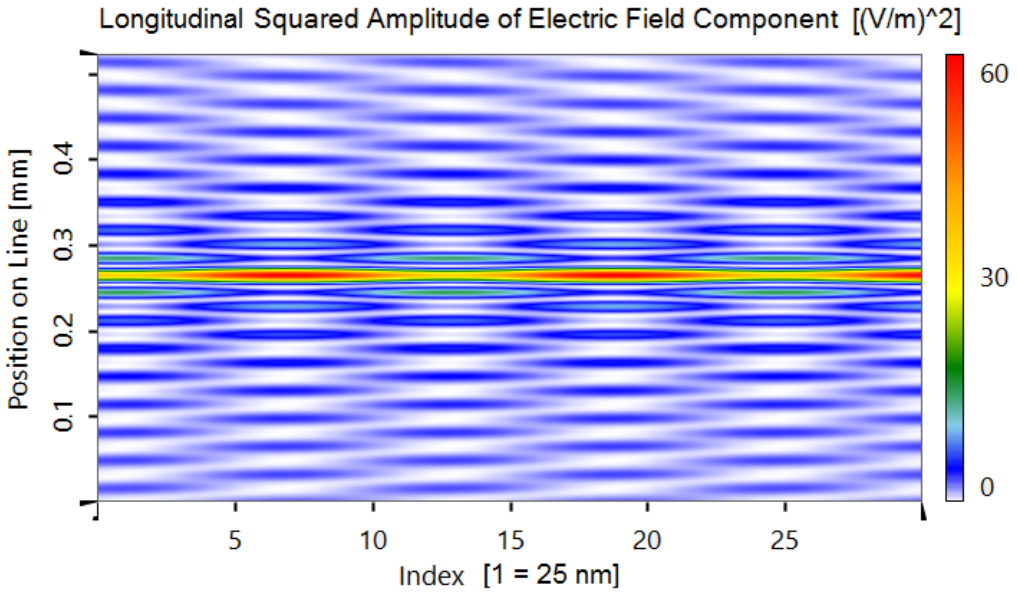

Figure 2.18: Simulation Bessel - Collinear Plane interference longitudinal intensity profile. Plane wave phase delay $0 - 1.5\ \mu m$.

Angular misalignment

Angular misalignment leads to the fringe pattern with a double frequency respectively to the common plane - plane interference of the same tilt *Fig. 2.20*. Image taken by the camera is an evidence of the special phase distribution noted before on *Fig. 2.16*.

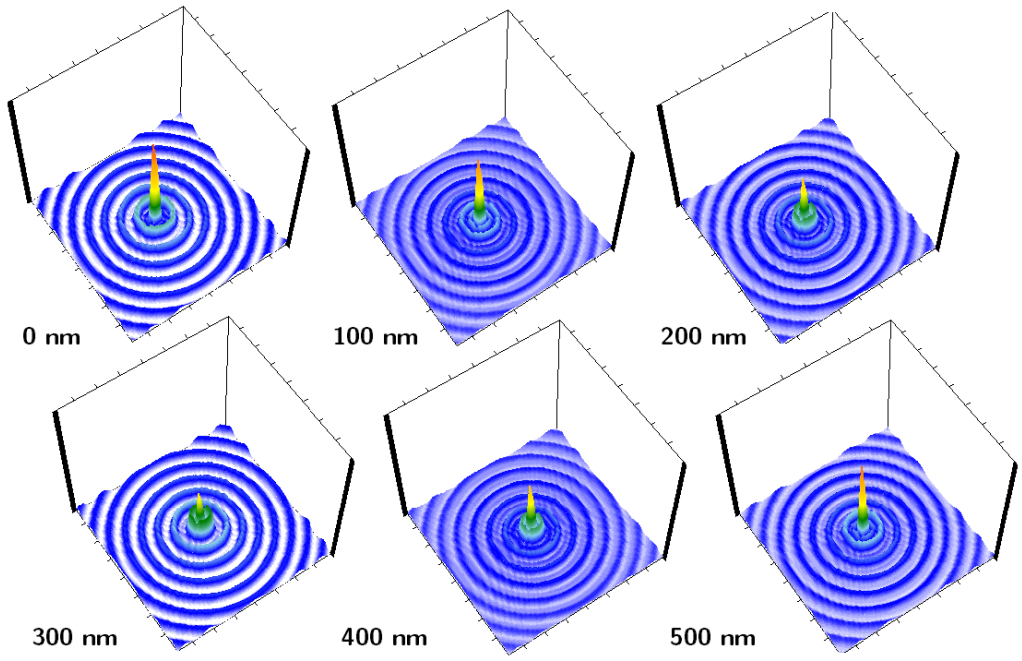

Figure 2.19: Simulation Bessel - Collinear Plane interference transversal intensity profile. Relative phase delay $0 - \lambda = 600nm$.

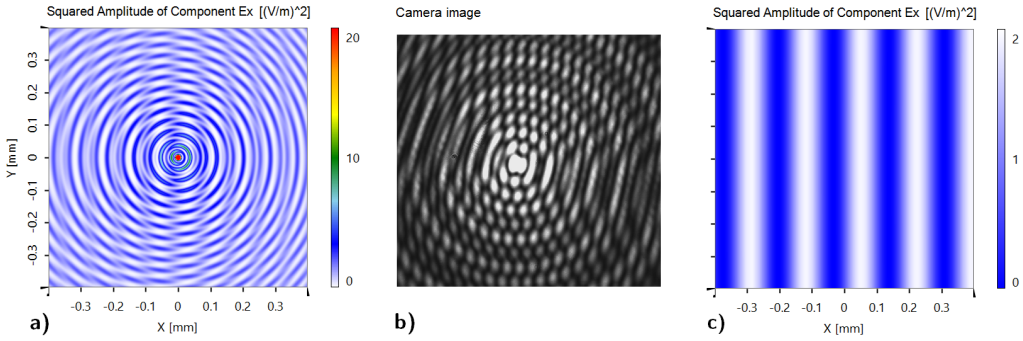

Figure 2.20: *a)* Simulation Bessel - Tilted Plane interference. *b)* Camera image of Bessel - Tilted Plane interference *c)* Simulation Plane - Tilted Plane interference with the same angular tilt.

Interference contrast

A contrast (visibility) of interference reveals the measure of intensity fluctuation. It shows the effect on the intensity of each electrical field onto resulting interference. In the case of spatially and temporally coherent waves with the same polarisation, we can write a term of ideal interference contrast dependent on the mutual intensity ratio.

$$\text{Contrast(ideal)} = \frac{2\sqrt{I_1 I_2}}{I_1 + I_2} \tag{2.6}$$

Plane wave intensity distribution is homogeneous. On the other hand in *Sec.2.1.2* we referred on a Bessel beam intensity profile which is far from homogeneous. Thus, the contrast of the interference will be coordinate dependent. The ratio between intensities of the plane wave and the Bessel beam predicts the part of the Bessel beam which will be influenced the most *Fig. 2.21*. The best overall contrast occurs at the ratio 92:8, which corresponds to the situation when the plane wave has the same intensity as the outer rings of the Bessel beam.

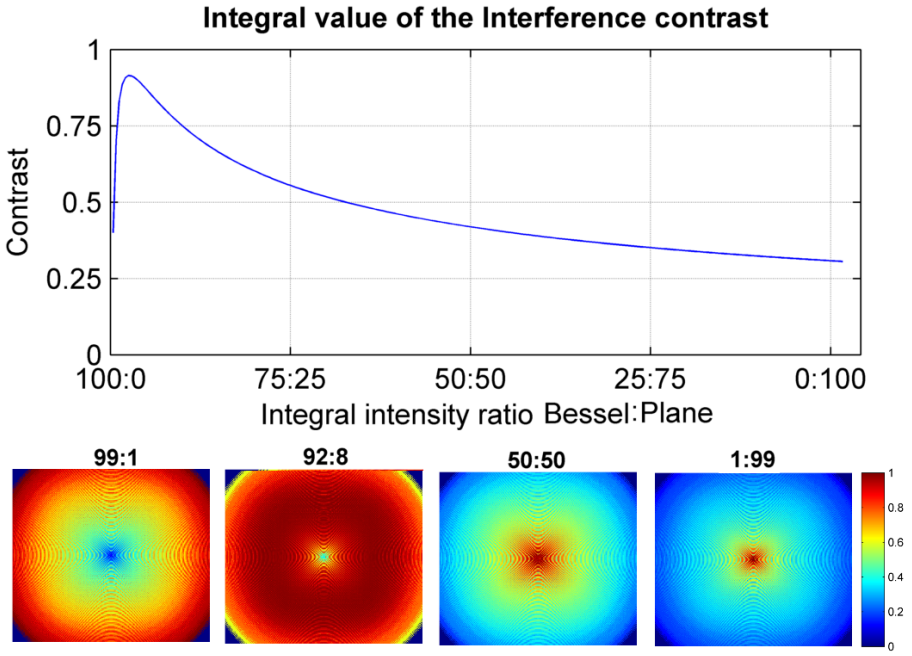

Figure 2.21: Integral value of the interference contrast for different Bessel:Plane intensity ratios. Coordinate dependant interference contrast.

Integral intensity fluctuation

The transversal interference pattern changes its character twice as often as in the case of plane - plane interference. This behaviour will be the most significant for the Bessel:Plane intensity ratio of 92:8 *Fig. 2.22*. Different ratios lead to a decrease of the contrast of the integral intensity fluctuations. Due to the Bessel beam transversal

intensity inhomogeneity, we can not avoid parts which will not interfere with the sufficient contrast, hence the contrast of the integral intensity fluctuations will be low. For the ratio 50:50 the phenomenon is almost unobservable - amplitude of integral changes are beaten by the bright core fluctuations.

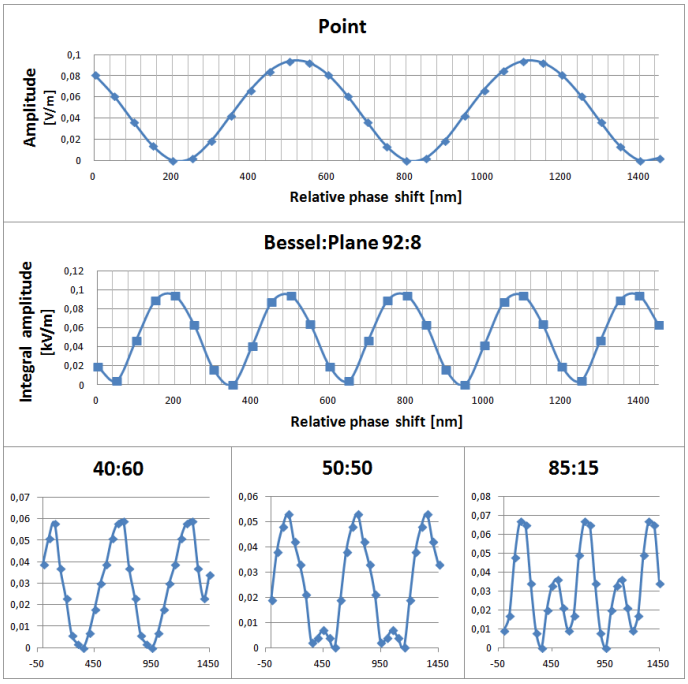

Figure 2.22: Simulation Bessel - Plane interference. Point amplitude fluctuation and Integral amplitude fluctuation for different input beams intensity ratio.

2.4.2 Experiment

The experimental set-up is a classical Mach - Zehnder interferometer with an axicon in one of its arm *Fig. 2.23*. The reference mirror is equipped by a piezo-actuator for accurate induce of a relative phase shift. The result is captured on the camera and further processed in MATLAB.

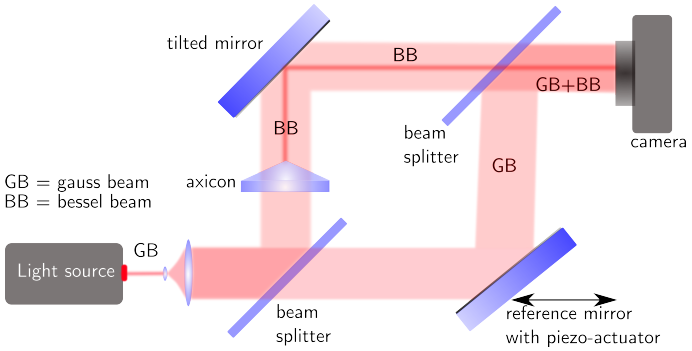

Figure 2.23: Modified Mach - Zehnder interferometer for the Bessel+Plane interference.

Measured results correspond with the simulated data. The integral intensity changes its value twice as often as the point intensity. The point intensity keeps changing within the period of the wavelength. That is a proof of potentially new concept of synthetic wavelength based on the proper light structuring.

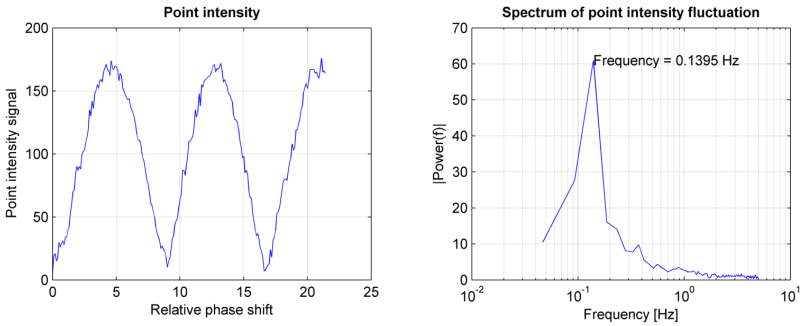

Figure 2.24: Measured Bessel Plane interference point intensity fluctuation while the relative phase shift is induced.

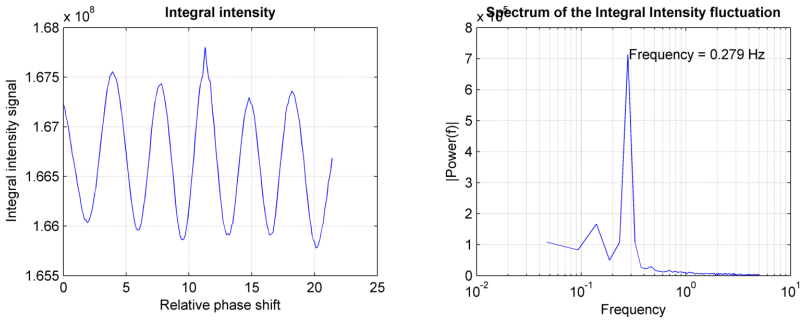

Figure 2.25: Measured Bessel Plane interference integral intensity fluctuation while the relative phase shift is induced.

2.5 Bessel - Bessel interference

Interference of two Bessel beams can provide another degree of freedom to our measurement *Fig. 2.26*. Relative phase shift and angular misalignment are the ones which we experienced even in the case of plane - plane interference. Additionally, due to the central symmetry of the Bessel beam, we can obtain another information about the offset of bright cores (or tips of cones in the spatially spectral domain). This kind of transversal shift can not be revealed in the case of plane waves where the intensity pattern is not subject to any change since plane waves are mathematically defined over the entire space.

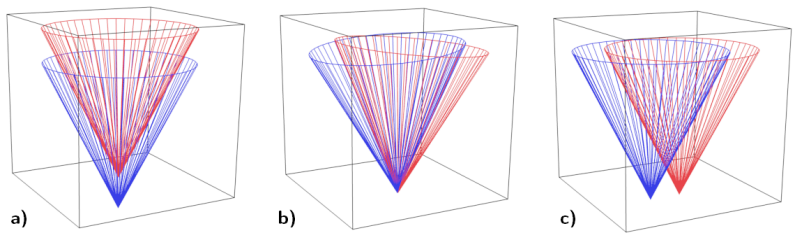

Figure 2.26: Interference of two Bessel beams. *a)* relative phase shift on the axis of propagation*b)* angular misalignment *c)* off-set of cone tips (bright cores)

2.5.1 Degrees of freedom

Relative phase shift

The first degree of freedom is relative phase shift on the axis of propagation. We made the simulation of two Bessel beams with inducing a relative phase shift $0 - \lambda$. The intensity of each part changes its value with sin dependence which is the same behaviour we observed in the case of plane - plane interference.

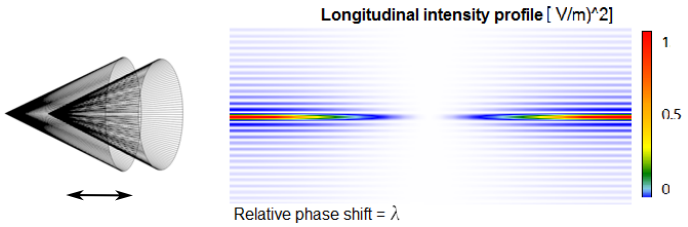

Figure 2.27: Simulation of the interference of two collinear Bessel beams with inducing relative phase shift $0 - \lambda$

Angular misalignment

The angular misalignment has a very similar effect to what we experienced in the case of plane - plane interference. For the cone tips laying in the same position interference fringes are straight with the frequency related to the mutual tilt.

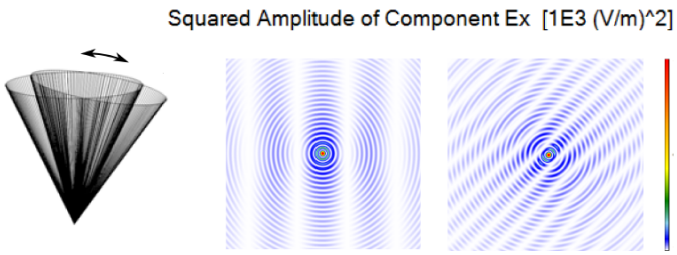

Figure 2.28: Simulation of Interference of two mutually tilted Bessel beams *a)* tilt in one dimension *b)* double tilt in both dimensions

Cone tips offset

A special feature of the Bessel beam interference is the possibility to distinguish a distance between bright cores. The area of intersection gives a rise to intensity fringes which number depends on the distance between bright cores and apex angles of Bessel beams. Origin of these fringes is not in the mutual tilt but in the wavefront dislocations; the same situation to the Bessel beam transversal profile where dark circles belong to spots where the phase is not defined. The first singularity and thus intensity minima occur while beams are at the distance where cores stop overlapping *Fig.2.29*. Other fringes appear with further distancing as more singularities from outer rings fits between cores. The position and number of fringes minima are given by the width of the Bessel beam rings and can be revealed from the Bessel function property. Λf gives us the distance of bright cores for relevant minima number k.

$$\Lambda f = 2J_0(x)\frac{\lambda}{\pi \sin \alpha} \tag{2.7}$$

where the $J_0(x)$ is the position of the Bessel function zeros.

Table 2.1: Bessel Function Zeros

k	1	2	3	4	5
$J_0(x)$	2.405	5.520	8.654	11.792	14.931

As a conclusion, the number of fringes between two interfering bright cores is related to the mutual distance d, apex angle α and the wavelength λ. If we assume the value of $\alpha = 2°$ and $\lambda = 633$, the first minimum $k = 1$ occurs at the distance $d \approx 28.5\mu m$ and the second $k = 2$ at the distance $d \approx 65.4\mu m$. However, if we concede larger apex angle 20°, the resolution increase ten times and the first minimum appears at the distance of $d \approx 2.85\mu m$. The number of minimums influences overall image, then it is quite easy to distinguish its number and thus, the transversal distance with the precision equals to Λf.

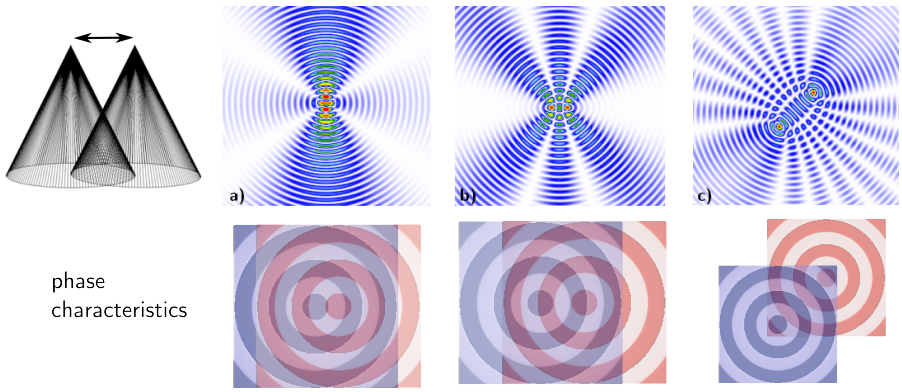

Figure 2.29: Simulation of tips offset of two interfering Bessel beams *a)* tips distance $20\mu m$ *b)* tips distance $50\mu m$ *c)* tips offset $100\mu m$ in both directions

2.5.2 Combination of misalignments

Relative phase shift + Angular misalignment

Relative phase shift with an angular misalignment leads to a fringe pattern moving such as in the case of plane - plane interaction.

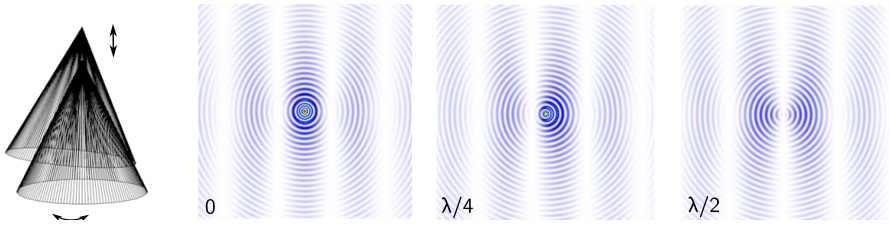

Figure 2.30: Simulation of the combination of angular misalignment and relative phase shift.

Relative phase shift + Cone tips offset

Combining relative phase shift with a cone tips offset we get pattern periodically changing its shape with a period equal to λ. When the relative phase shift equals to $\lambda/2$ the intensity pattern has an inverse composition and the bright cores are at minimums. Point intensity value has the same property of sinusoidal profile as in the case of plane - plane interference.

Angular misalignment + Cone tips offset

By the tips offset the pattern loose its symmetry in one direction. Therefore, we obtain different results when directions of cone axis aim away from or to each other. The first direction "from" results in the open fringe pattern *Fig.2.32a)*, the second while axis are aiming "to" each other fringes are closed *Fig.2.32d)*. By inducing a tilt into second dimension we obtain spiral-like shape pattern *Fig.2.32b),e)*. The

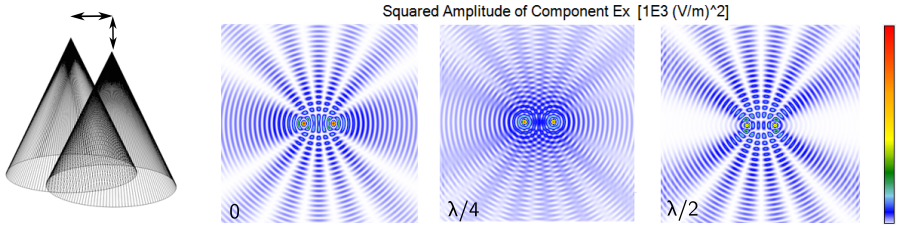

Figure 2.31: Simulation of the combination of tips offset and relative phase shift.

fringe pattern periodicity depends on the mutual angle *Fig.2.32b),c)*. The number of fringes between bright cores, which then creates closed or open fringes, is given only by their distance (not by the mutual angle)*Fig.2.32f)*.

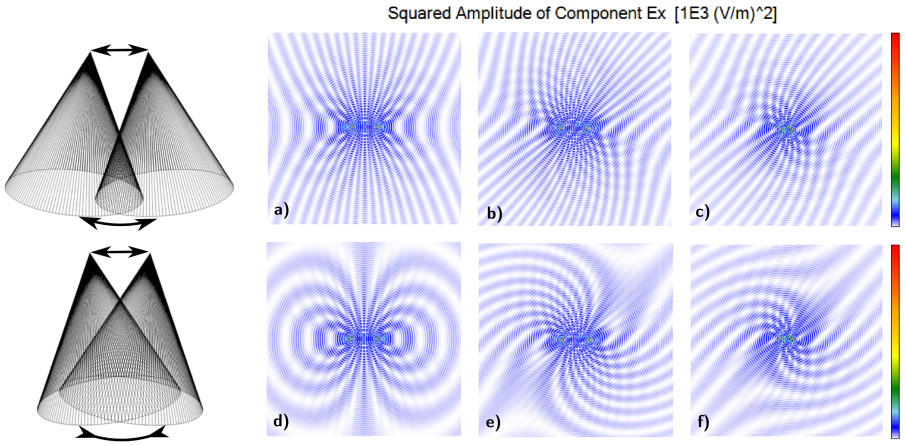

Figure 2.32: Simulation of the combination of tips offset and angular misalignment.

Angular misalignment + Cone tips offset + Relative Phase shift

By moving with all three degrees of freedoms we got the superposition of above-shown patterns. This interaction stores all previously noted information which does not influence each other: relative phase shift, mutual tilt and the distance of the bright cores.

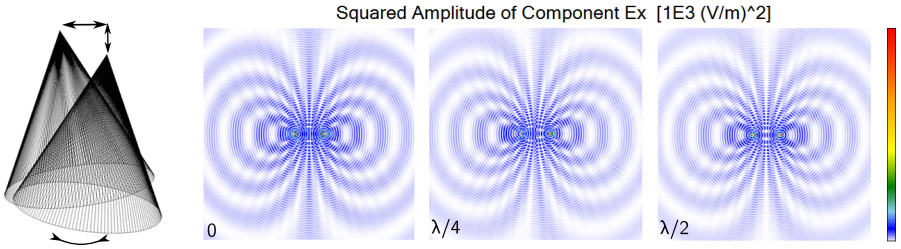

Figure 2.33: Simulation of the combination of tips offset, angular misalignment and relative phase shift.

2.5.3 Experiment

Experiment with two Bessel beams interference was performed by the Twymann - Green set-up modified by the axicon placed at the input. By positioning and tilting of mirrors we can obtain above described situations *Fig.2.34*.

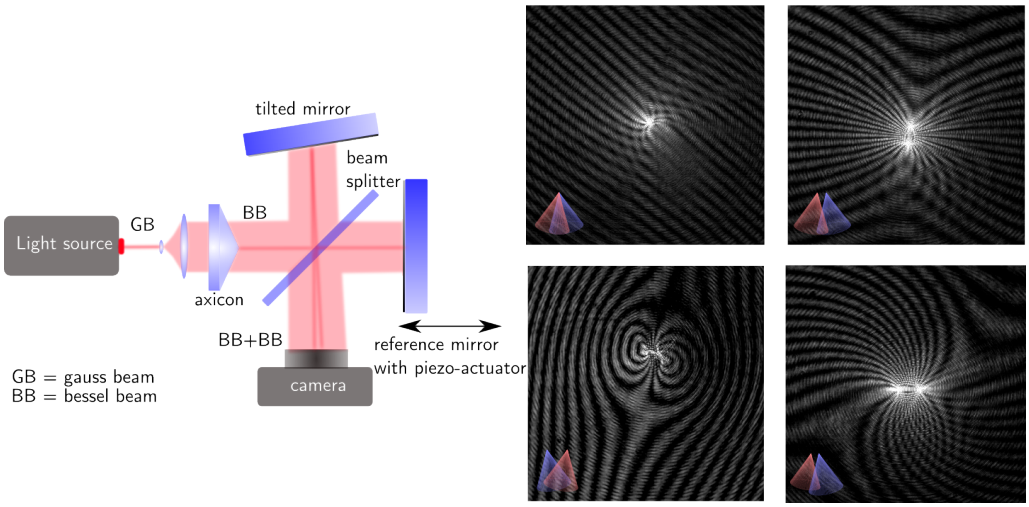

Figure 2.34: Experiment of the interference of two Bessel beams.

2.5.4 Model situation of absolute distance measurement

In the previous section, we referred on properties of two Bessel beams interference. In the following we will propose the model situation of utilisation above stated assumptions for precise positioning or alignment. The interferometry in conventional arrangement yields only relative distance measurements. Consequently, it cannot provide answers for the distance between the arbitrary datum to a point. However, that kind of information is reachable by the absolute length interferometry. Currently, the problem is still seen as highly specialist and with high demands on environmental conditions or with the responsibility of maintaining length standards. The state of the art methods uses synthetic wavelength approach or the frequency scanning interferometry [21]. Both are suffering some limitations such as sensitivity to distortions, the speed of the measurement or a dynamic range of measurable distances. Every advancement which can provide sub-millimetre precision over the distance up to tens of centimetre is desirable.

Our solution consists of using simple geometry, which is the principle to a certain extent prevented to the Gaussian beam. Since the Gaussian beam does not keep its width while propagates it is not predetermined for a very precise tracking. Further, while two Gaussian beams interfere, we can distinguish only the mutual tilt or relative phase delay, not the mutual offset over the transversal plane.

Concept

The concept is based on the previously noted behaviour of two interfering Bessel beams. Thanks to the thin filament of Bessel beams we are able to trace the direction of the beam much more precisely than in the case of conventional beams. Further, we can simultaneously profit information from the wave interference properties. On the following figure is the scheme of our concept *Fig.2.35.*

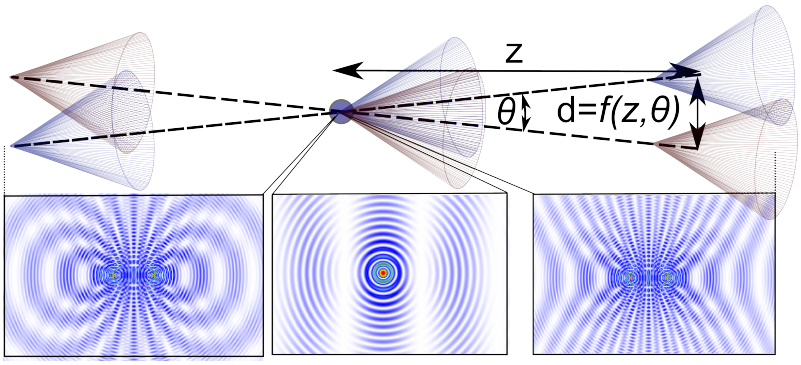

Figure 2.35: Concept of absolute distance z measurement with two interfering Bessel beams

Two mutually tilted off axis Bessel beams are intersecting at the datum point. Before the datum point, the intensity pattern appears with distanced cores and closed fringes raising from minimums between; just in the point cores merge and fringes are straight with periodicity related to their mutual tilt θ; after the datum point cores are separated again and fringes are open. That provides us with the information about the position of the datum point with the precision related to the distance z_{1min} where the first minimum occurs between two separated cores *Sec.2.5.1.*

First, minimum occurs at $d = 2J_0(k_1, x)$ its position z_{1min} is the factor related to the mutual tilt θ, the radius of the central core $J_0(k_1, x)$ so the apex angle of Bessel beams α and the wavelength λ (from *Eq.1.25*). The distance can be revealed by trigonometric functions.

$$z_{1min} = \frac{J_0(k_1, x)}{\tan(\theta/2)} \tag{2.8}$$

Bessel beams with larger apex angle exhibit smaller central core and thus the resolution is better. However, their dynamic range is limited by the relatively smaller depth of focus z_{max}. Better resolution can be achieved by Bessel beams directed from larger angle θ, which leads to faster z_{1min} appearance. On the other hand angles larger than 3° leads to the fringe pattern with the period smaller than the resolution limit of a standard camera and thus we might loose the advantage of wave properties.

With the axicon angle of $\alpha = 2°$ we can reach the resolution up to $1mm$ while beams enclose angle $\theta = 2°$. Simulation of the pattern envelopment is proposed at *Fig.2.37.*

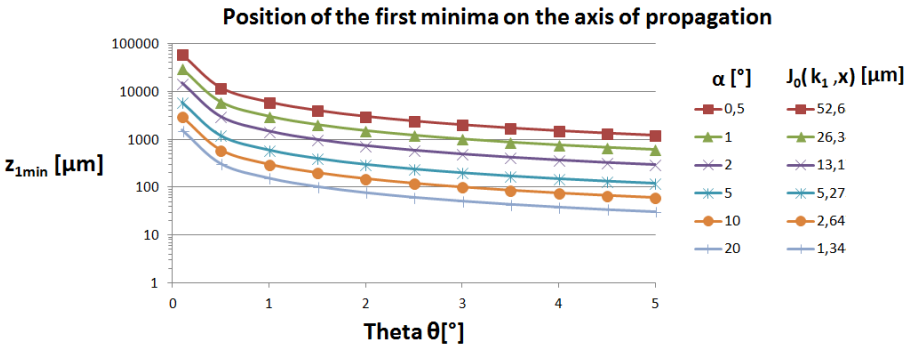

Figure 2.36: The position of the first minimum z_{1min} related to the axicon angle α of Bessel beams and their mutual propagation angle θ.

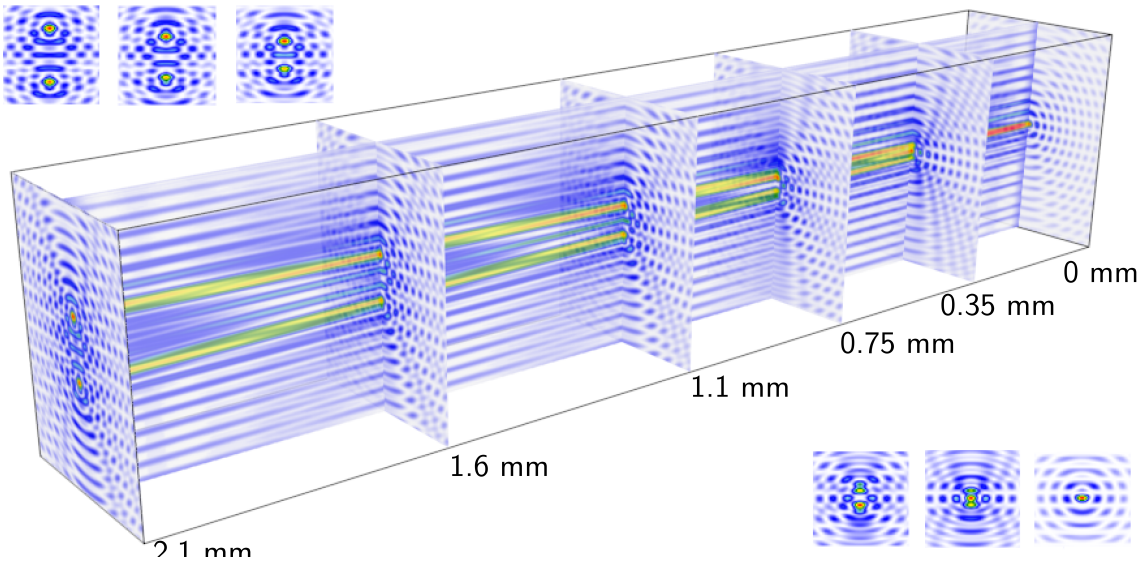

Figure 2.37: Simulation of absolute distance z measurement with two interfering Bessel beams.

2.6 Structured field + Plane interference

Bessel beams are not only fields which yield special phase property. The constant phase with the phase shifts is characteristic for fields that arise from the interference of constantly tilted waves. For example, simple interference pattern made by two waves gives rise to slices in space where adjacent fringes are shifted by π. Or the interference of four waves creates a chessboard-like transversal pattern where adjacent blocks yield the π phase delay *Fig.2.38*.

It is not that surprising that while we add another dimension into our measurement that we obtain more precision. However, while we increase the angle of interfering beams to the value when the pattern period is smaller than the resolution limit of a detector, we might start to assume the dual phase character as the 1D property of the field.

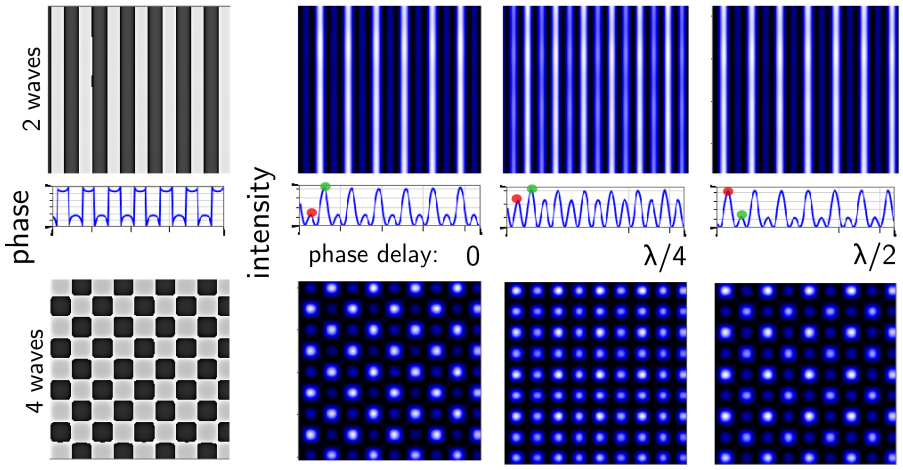

Figure 2.38: Interference of structured fields with plane wave.

Chapter 3

Long range non-diffracting beams

The property of non-diffracting spreading over the long distances is without doubt very promising for many applications in free-space optics. Beam spreading disqualifies optical approach in long distance positioning or alignment which is the subject of vivid study for precise alignment of long-distance experiments in CERN.

Conventional generators of Bessel beams, based on an annular slit or an axicon, offers a range of existence usually up to a few metre or less. The limitation comes from an origin of a generation - the geometrical property and the finiteness of participating waves. Thus, there has been a call for novel approaches overcoming these issues and enabling generation of the narrow beam over the long distances.

3.1 Long range non-diffracting beam generation

3.1.1 Axicon generalization

The first idea of conical axicon reflects consideration of providing conical k-vector spectrum. It is consideration coming purely from the concept of geometrical optics and it results in a Bessel beam of non-homogeneous intensity distribution over the axis of propagation (even in the perfect case). A different point of view was given by Sochacki and Kotodziejczyk [23] who developed a theory based on the assumption of energy conversion. Physically, their equation reflects that the two-dimensional power density of incoming beam is being transformed into the one-dimensional axis density. That leads to the definition of more general axicons which can perform unified intensity over the beam existence by setting out conditions on surface geometry. It also initiated more complex view of non-diffracting beams creation by an architecture of generator in order to design output wavefront [24] [25]. The effort of these circles was more concerned about the production of a Bessel beam in short distances equivalently to that produced by axicons. However, the stated theory could also serve as description of long range non-diffracting beams [26] [27] [28].

3.1.2 Non-diffracting beams generated by a spherical aberration

Independently on previously noted studies there was published work on the generation of the beam keeping its narrow width while propagates over large distances [29] [30]. Proposed solution implements negative spherical aberration into Galilean type telescope *Fig.3.1.*(*Positive* spherical aberration means peripheral rays are bent too much. *Negative* spherical aberration means peripheral rays are not bent enough.) An important feature of the non-diffracting beam existence is the radial symmetry of contributing beams and the constant angle relative to the axis of propagation. The first condition is fulfilled thanks to the radial symmetry of spherical aberration; the second condition is reached in the area, where rays from the outer part of distorted wavefront converge to the optical axis. Results proposed in [30] promises beam which maintain its width of 20 cm over the distance up to ten kilometres!

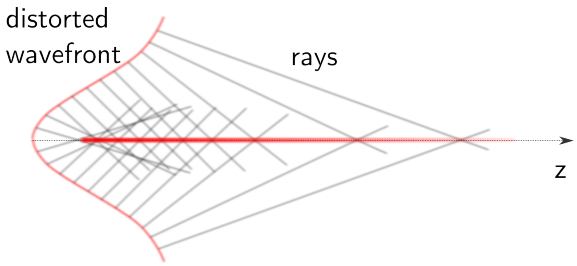

Figure 3.1: Concept of the long range non diffracting beam generation

3.2 Design of long range non-diffracting beam generator

3.2.1 Phase function of ND generator

We can state the proper phase function $\Theta(\rho)$ for the element generating non-diffracting beam over the desired distance with a linear increasing intensity (such as a case of the axicon we examined in the previous chapter). Assuming a plane wave input to the element we can write [23]:

$$\Theta(\rho) = -\frac{\left[\left(1-\frac{z_2^2-z_1^2}{R^2}\right)r^2+z_2^2\right]^{1/2}}{1-\frac{z_2^2-z_1^2}{R^2}} \tag{3.1}$$

where ρ is the distance from the optical axis, R is the radius of element,z_1 and z_2 gives the range of non-diffracting beam existence. The equation is evaluated on the *Fig.3.2* for values $z_1 = 0$, $z_2 = 50cm$, $R = 13.2$.

It shows the ideal phase retardation function for the generator with radius $R = 13.2\ mm$ which create the non-diffracting beam of the same width at the range

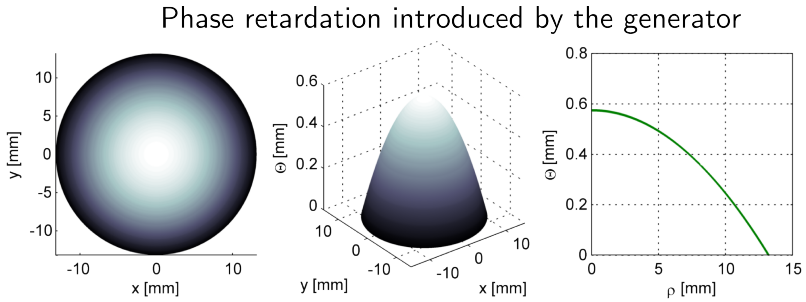

Figure 3.2: Phase retardation function of the non-diffracting beam generator for constant width beam in $0 - 50$ *cm.(rendered in MATLAB)*

$z_1 = 0cm$, $z_2 = 50$ cm. The character of the function will not change with the range, even for the range $100 - 200$ m we would obtain the function similar to *Fig.3.2* only with the different range of values. For further distances function yields a smaller range of values which reflects the condition under which non-diffracting beam exist - rays must be convergent toward the optical axis and while we assume rays are directed perpendicularly to the retardation function, then for long ranges the sample influence has to yield small angles.

Realisation of such function has some limits. For short distances, the range of values is in the order of millimetres, however with increasing distance the range decrease as fast. For hundreds of metres, we would need a function on micrometre scale with the precision up to the fraction of λ. Thus, it is more convenient to use holographic approach, graded-index (GRIN) lenses or, as was pointed before in *Sec.3.1.2*, the effect of aberrations.

3.2.2 Wavefront distortion described by Zernike polynomials

Often, it is convenient to characterise wavefront data in polynomials. Zernike polynomials have been often used for this purpose since they have a form similar to distortions made by the real optical systems [31]. They form a complete set, they are orthogonal over the continuous unit circle and all their derivatives are continuous. They also yield rotational symmetry and thus they can be fully characterised by two numbers describing radial and angular symmetry.

Analysis of the wavefront consists of an assignment of weight coefficient $[\lambda]$ to polynomials. By the sum of polynomials with the relevant coefficients, we can reconstruct the wavefront. This analysis is very convenient as it simplify the wavefront characterization and it might serve as a useful tool for non-diffracting generator design.

Spherical aberration and Defocus

Aberrations with rotational symmetry are of particular importance for the generation of non-diffracting beams. Spherical aberration occurs as the different refraction of rays near an edge of optical element than those at the centre. The effect is proportional to the fourth power of the diameter and inversely proportional to the third

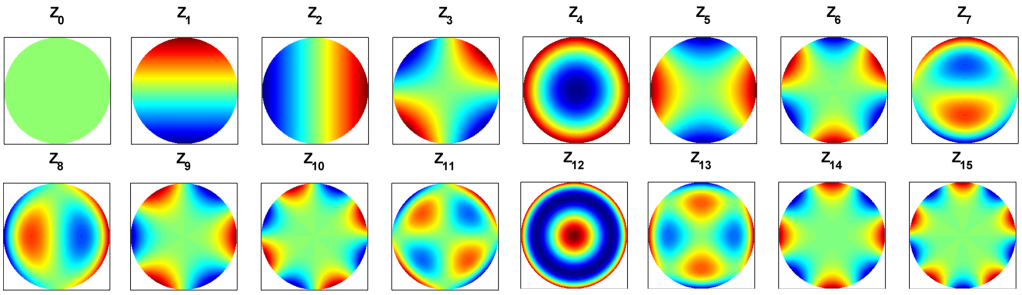

Figure 3.3:
Z_0 Piston, Z_1 x-tilt, Z_2 y-tilt, Z_3 Astigmatism, Z_4 **Defocus**, Z_5 Astigmatism, Z_6 Trefoil, Z_7 Coma, Z_8 Coma, Z_9 Trefoil, Z_{10} Quadroil, Z_{11} 4th order Astigmatism, Z_{12} **Spherical Aberration**, Z_{13} 4th order Astigmatism, Z_{14} Quadroil, Z_{15} Pentafoil, *(rendered in MATLAB)*

power of the focal length [31]. *Fig.3.4* shows the evaluation of low-order aberrations with the radial symmetry which are the most significant case in a simple element.

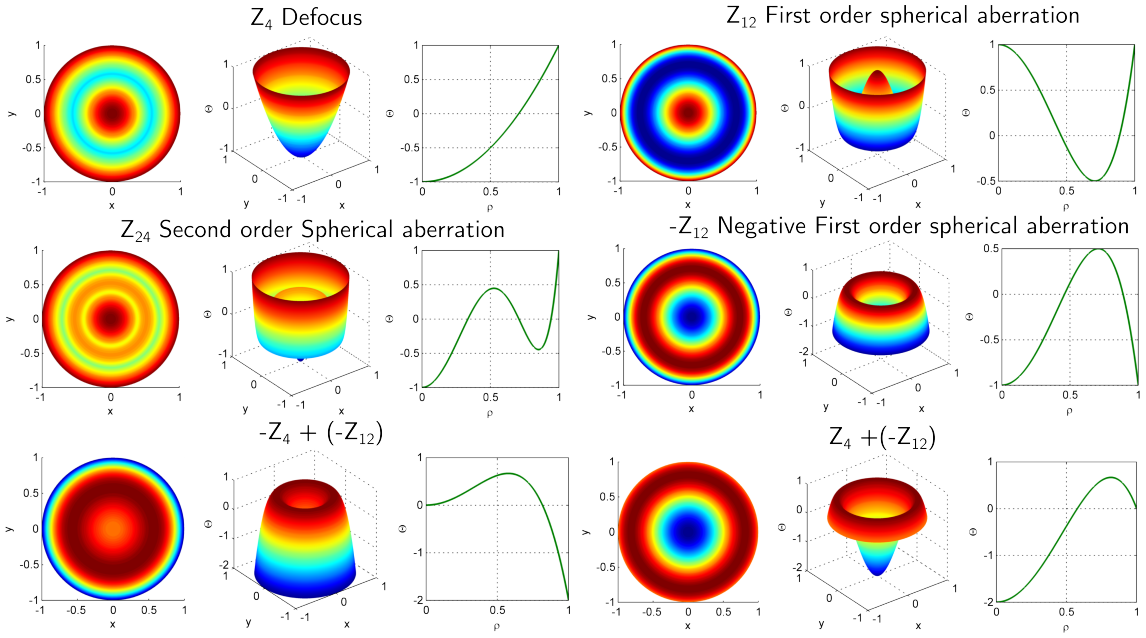

Figure 3.4: Zernike polynomials with the rotational symmetry, *(rendered in MATLAB).*

A choice of suitable aberration and its weight can be guided by *Eq.3.1* where we got an equation giving into relation curve of phase delay with the distance of ND beam existence. We could assume that highly curved parts of functions will be responsible for the beam closer to the generator; on the other hand, these with a lower angle to the axis will create the further part of the beam.

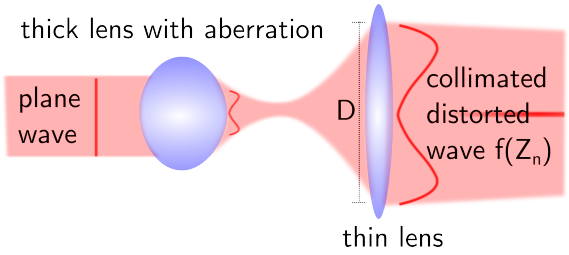

Figure 3.5: Scheme of long range non diffracting beam generator

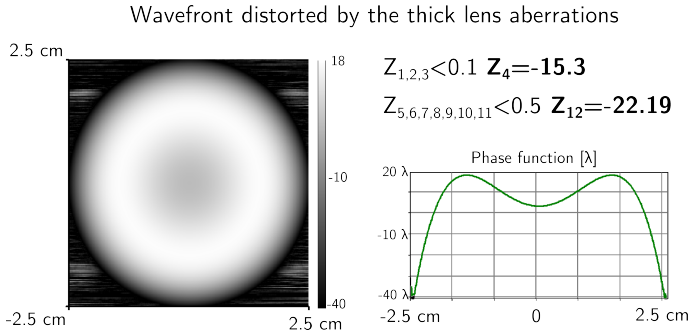

Figure 3.6: Wavefront outgoing from the non-diffracting beam generator.

3.3 Long range non-diffracting beam generator

The most common wave distortion induced by a spherical lens can be described as a combination of *defocus* and *negative spherical aberration*. Long range non-diffracting beam generator actually collimates and enlarge distorted wavefront to a diameter D. Parameters of the generator can be then characterised by coefficients of Zernike polynomials describing wavefront distortion and the diameter D of the whole field (not a bright core).

Diameter D is given by collimating lens which we assume as the aberration-free sample. Induced distortion can be experimentally measured by a wavefront sensor such as Shack-Hartmann. Further, we can also make a simulation (or get one straight from a vendor) and find out coefficients virtually.

3.3.1 Simulation

Evaluation of the first sample

The simulation of optical elements with keeping its wave character is still computationally demanding task. However, once we evaluate Zernike coefficients of the wavefront outgoing from the sample, we might be able to simulate the whole beam in a fraction of the time. From the model of the thick spherical lens available in our lab we obtained result shown in *Fig.3.6*. As we expected, the highest coefficients are of radially symmetrical aberrations: defocus and first order spherical.

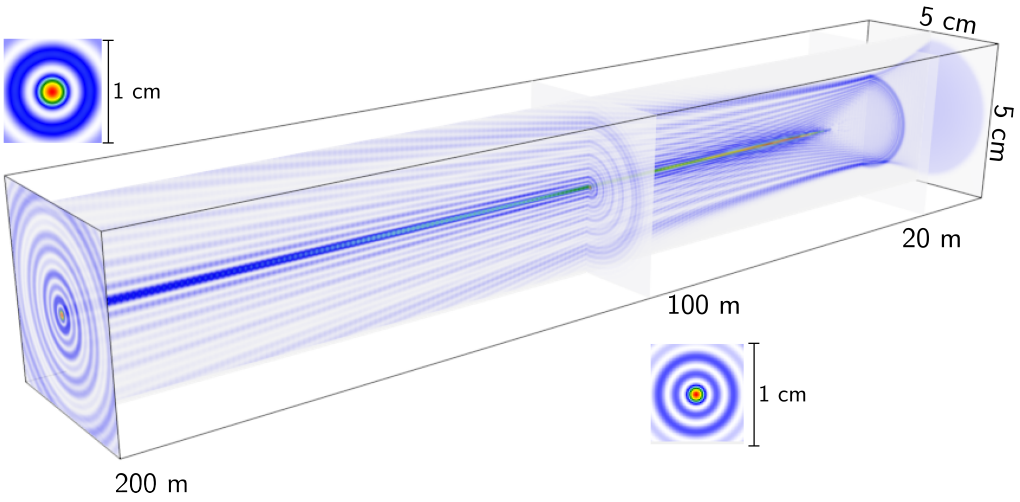

Figure 3.7: Long range non-diffracting beam simulation

Propagation of the beam with distorted wavefront

With knowledge of the wavefront, we can define its behaviour during propagation *Fig.3.7*. The bright core first occurs at the distance of approximately 30 m which corresponds to contributions of outer parts. Then the beam is "fed" by the milder central part and thanks to that we might be able to observe the central bright core which keeps its width less than 5 mm in 200 m!

3.3.2 Experiment

We performed experiments with the generator of the non-diffracting beam with sufficient results coinciding with simulations. It was measured a diameter of less than 5 mm in the long corridor at the distance of approximately 200 m.

We captured an image of the non-diffracting beam from the defocused generator (which illustrate faster envelopment of the beam) and profile of the Gaussian beam over the same distance *Fig.3.8*. It is clearly visible that even with significant misalignment of the system our beam is much less divergent than the casual one.

3.4 Long range non-diffracting beams conclusion

Currently, there are known several ways how to generate beams which are subject to much less spreading than casual Gaussian beams. Such property has been used for a free space optics communication, however, it has not aroused too much attention. We believe, this beams might bring advantage to any field where the beam spreading is limiting. For example, increasing the width of a Gaussian beam stand in a way of long distance light position tracking which plays a huge role in physical experiments where the high precision over the entire experiment is needed, such as in particle

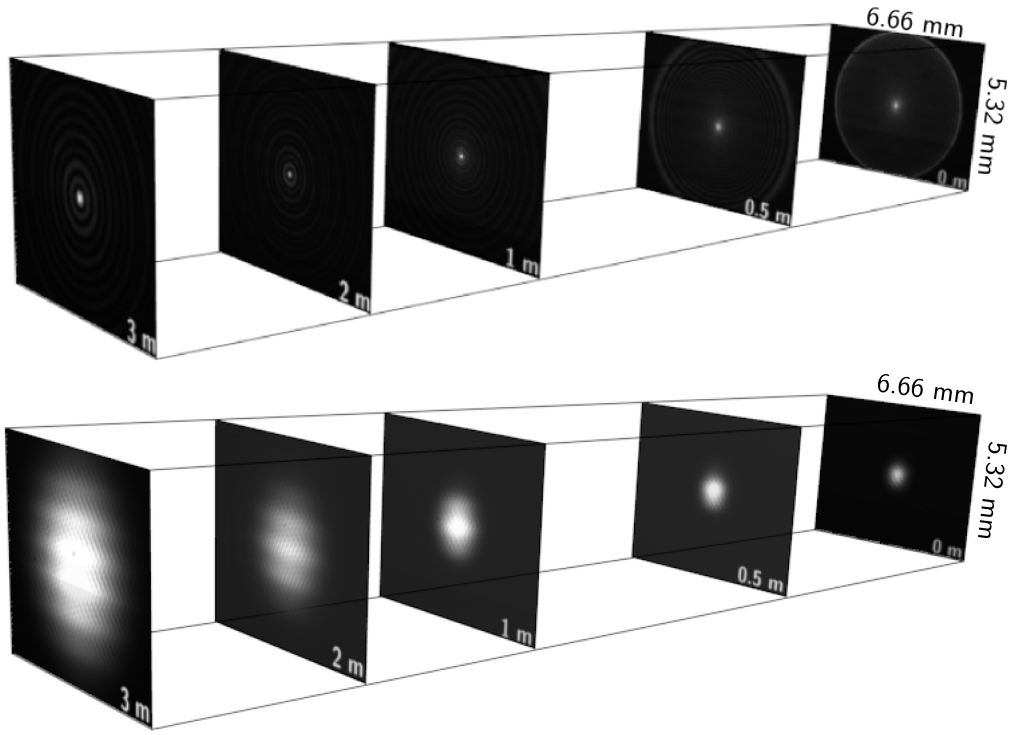

Figure 3.8: Camera image showing long range non-diffracting beam in comparison with Gaussian beam

accelerators. With a price of outer rings, we can produce a bright core propagating with a diameter less than 5 mm over the hundreds of metres, which is a great achievement compared to casual beams. Further, outer rings may serve for a more accurate determination of the centre and so it may be a great tool for direction tracking.

Conclusion

Submitted thesis analyses possibilities of the novel shape of light beams in optical metrology. We referred on a few unconventional properties which were physically explained and investigated by simulations in the software VirtualLab Fusion and supported by experiments.

In the first chapter we built up the theoretical background based on current knowledge in the field. We demonstrated the interesting property of non-divergent propagation of the Bessel beam by putting him side by side with the conventional Gaussian beam.

The second chapter investigate very little explored field of non-diffracting beams interference. We revealed special phase characteristic of Bessel beams which plays a significant role in the interference phenomena.

- **Bessel - Gauss interference:** For the interaction of a Bessel beam with a Plane wave (or Gaussian beam) we found out, that **the periodicity of intensity changes is half** compared to ordinary plane-plane interference. This is the interesting approach to increase of precision by factor of two without using any dynamical method.
- **Bessel - Bessel interference:** Due to the central symmetry of Bessel beams we can profit from **another degree of freedom** - central part offset. We made simulations showing the transversal intensity pattern behaviour within changing of all degrees of freedom. We proposed how to use this additional information in absolute distance measurement.

The last chapter is devoted to long-range non-diffracting beams. It is very desirable to find a way how to produce beam with properties of Bessel beams over the long distances. One of the proposed methods is by means of spherical aberration of a collimating system. We investigate such generators with the theory well established in the field of optical imaging using wavefront description by Zernike polynomials. This method proved to be very helpful for its simplification and physical insight. It also brings significant improvement for the beam simulation.

Bibliography

[1] Saleh B. E. A., Teich M.C., *Základy fotoniky*; I,II , MATFYZPRESS, Praha, 1994-95

[2] Hernández-Figueroa H., Zamboni-Rached M., Recami E., *Non-Diffracting Waves: An Introduction,*; 2013, ISBN-13: 978-3527411955

[3] Goodman, J. W. *Introduction to Fourier optics.* 2nd ed. New York: McGraw-Hill, 1996. ISBN 0070242542.

[4] F. Wyrowski, H. Schimmel, *Electromagnetic optical engineering - shaping light through design*, Photonik international 2008/1, p.80-83.

[5] F. Wyrowski and Ch. Hellmann, *Geometrical Optics Reloaded – Physical optics modelling with smart rays*, Optik& Photonik, 43-47, 5/2015;

[6] Durnin J., *Exact solutions for nondiffracting beams. I. The scalar theory.*; JOSA A, Vol. 4, Issue 4, pp. 651-654 (1987)

[7] Durnin, J., J. J. Miceli and J.H. Eeberly, *Diffraction-free beams*, Phy. Rev. Lett., 58, 1499-1501.(1987)

[8] Bouchal, Z. *Nondiffracting optical beams: physical properties, experiments, and applications,* Cz. J. Physics, 53 (7) pp. 537–624, (2003)

[9] D. McGloin, K. Dholakia *Bessel beams: diffraction in a new light* Contemporary Physics, Vol. 46, No. 1, 15 – 28, Jan–Feb (2005)

[10] J. McLeod, *The Axicon: a new type of optical element,* J. Opt. Soc. Am. 44 592–507, (1954)

[11] O. Brzobohatý, T. Čižmár, P. Zemánek, *High quality quasi-Bessel beam generated by round-tip axicon* Opt. Express 16, 12688-12700 (2008)

[12] N.Chattrapiban, E. A Rogers, D. Cofield, R. Roy *Generation of non-diffracting Bessel beams by use of a spatial light modulator* Optics Letters, Vol.28, No.22, (2003)

[13] J. A. Davis, E. Carcole, D. M. Cottrell *Nondiffracting interference patterns generated with programmable spatial light modulators* APPLIED OPTICS, Vol. 35, No. 4, (1996)

[14] M. Erdelyi, Z. L. Horvath, G. Szabo , and Zs. Bor, F. K. Tittel, J. R. Cavallaro, M. C. Smayling *Generation of diffraction-free beams for applications in optical microlithography* J. Vac. Sci. Technol. B 15(2), (1997)

[15] X. Zhu, A. Schülzgen, L. Li, N. Peyghambarian *Generation of controllable nondiffracting beams using multimode optical fibers* App. Phy. Lett., 94, 201102, 2009

[16] Lv Q., Z. Zhai, X. Zhu, Z. Xu, X. Wang. *Interference patterns of two non-diffracting beams.* Optics Communications [online]., 285(6), 960-964 [cit. 2016-04-25]. DOI: 10.1016/j.optcom.2011.11.079. ISSN 00304018. (2012)

[17] S. Chavez-Cerda, E. Tepichin, M. A. Meneses-Nava and G. Ramirez *Experimental observation of interfering Bessel beams*, Vol.3, No. 13, OPTICS EXPRESS 524, (1998)

[18] D. McGloin, V. Garcés-Chávez, and K. Dholakia *Interfering Bessel beams for optical micromanipulation*, , Vol. 28, No. 8, OPTICS LETTERS, (2003)

[19] T. Cizmar, V. Garcez-Chavez, K. Dholakia and P. Zemanek, *Optical trapping in counter-propagating Bessel beams*, Proceedings of SPIE Vol. 5514 SPIE, doi: 10.1117/12.557188, (2004)

[20] M. Fortin, M.l Piché and E. F. Borra, *Optical tests with Bessel beam interferometry*, Vol. 12, No. 24, OPTICS EXPRESS 5887, (2004)

[21] K. Alzahrani, D. Burton , F. Lilley, M. Gdeisat, F. Bezombes, and M. Qudeisat , *Absolute distance measurement with micrometer accuracy using a Michelson interferometer and the iterative synthetic wavelength principle*, / Vol. 20, No. 5 / OPTICS EXPRESS 5682 (2012)

[22] Čižmár, T. *Optical traps generated by non-traditional beams.* Brno, Ph.D. thesis. Masaryk University. Supervisor: Pavel Zemanek.2006

[23] J. Sochaki, A. Kolodziejczyk, Z. Jaroszewicz, and S. Bará, *Nonparaxial design of generalised axicons*, Appl. Opt., vol. 31, no. 25, pp. 5326-5330, 1992.

[24] A. Burvall, K. Kołacz, Z. Jaroszewicz, and A. T. Friberg, *Simple lens axicon*, App. Opt. Vol. 43, No. 25, 2004

[25] Z. Jarosewitz, J. Morales, *Lens axicons: systems composed of a diverging aberrated lens and a converging aberrated lens*, J. Opt. Soc. Am. A 16, 191–197 (1999).

[26] L. A. Ambrosio, M. Zamboni-Rached, and H. E. Hernandez-Figueroa, *Overcoming diffraction in FSO systems using (GRIN)axicons for approximating the longitudinal intensity profiles,* J. Lightwave Technol.29, 2527–2532 (2011).

[27] Zamboni-Rached M, Assis MC, Ambrosio LA., *Diffraction-resistant scalar beams generated by a parabolic reflector and a source of spherical waves.* Appl Opt. ;54(19):5949-55, 2015

[28] K. Wang, L. Zeng, C. Yin *Influence of the incident wave-front on intensity distribution of the nondiffracting beam used in large-scale measurement* Optics Communications 216, 99–103, (2003)

[29] T. Aruga, *"Generation of long-range nondiffracting narrow light beams",* Appl. Opt., vol. 36, no. 16, pp. 3762-3768, 1997

[30] T. Aruga,H. Kunimori, *"Nondiffracting Light Beams for Long Ranges",* Journal of the National Institute of Information and Communications Technology Vol.51 Nos.1/2, 2004

[31] MALACARA Daniel, *Optical Shop Testing, 3nd Edition.*; Hoboken, N.J:Wiley Interscience, 2007, ISBN 978-047-0135-969.;